Global and Planetary Change 171 (2018) 273–292

Contents lists available at ScienceDirect

Global and Planetary Change

journal homepage: www.elsevier.com/locate/gloplacha

Fluid composition changes in crystalline basement rocks from ductile to brittle regimes

Irene Cantarero[a,*], Gemma Alías[a], David Cruset[a], Eloi Carola[b], Pierre Lanari[c], Anna Travé[a]

[a] Departament de Mineralogia, Petrologia i Geologia Aplicada. Facultat de Ciències de la Terra, Universitat de Barcelona (UB), C/Martí i Franqués s/n, 08028 Barcelona, Spain
[b] Gas Natural Fenosa, Av. San Luís 77, 28033 Madrid, Spain
[c] Institute of Geological Sciences, University of Bern, Baltzestrasse 1+3, CH-3012 Bern, Switzerland

ARTICLE INFO

Keywords:
Ductile deformation
Brittle deformation
Fluid flow
Relay zone
Crystalline Palaeozoic basement
Catalan Coastal Ranges

ABSTRACT

The relationships between deformation and fluid flow have been investigated in the Paleozoic basement of an isolated horst of the Catalan Coastal Ranges. A structural, petrological and geochemical study has been performed in a complex fracture network that resulted from a long-lived tectonic history (from Carboniferous to Miocene).

Nine fracture types, developed from a ductile regime in the greenschist facies to a shallow brittle regime, have been characterized in order to establish P, T and fluid compositions during the evolution of the horst. Syn-cleavage and late-cleavage quartz veins (qtz$_1$-chl$_1$ ± mu and late qtz$_2$-chl$_2$-dol$_1$) formed during the Hercynian ductile deformation. These minerals precipitated from metamorphic fluids, possibly evolved from seawater, at temperatures between 240 and 340 °C. En-echelon albite vein arrays (ab-qtz$_3$-chl$_3$ ± ti-an) and NE-SW normal faults generating breccias mark the change from ductile to brittle, from compression to extension and from a closed to an open hydrologic regime. This paragenesis precipitated from the mixing of metamorphic and magmatic fluids at temperatures between 180 and 290 °C during the early Permian extension. Dolomite veins (dol$_2$-chl$_4$-qtz$_4$), precipitated at 210–280 °C from the mixing of previous fluids with hypersaline oxidizing external brines, possibly during the late stage of the early Permian extension. Reverse faults and calcite veins (Cc1-ba) formed either during the Paleogene compression or during the Langhian to early Serravallian minor compression. Calcite and barite precipitated from meteoric or marine waters in an open hydrological system at temperatures below 50 °C. The Miocene extension is represented by NE-SW normal faults with fault gouges and NNW-SSE normal faults cemented by calcite 2 that precipitated at temperatures below 50 °C from meteoric fluids in an open basin-scale hydrological system.

The studied horst was part of a relay zone between two segments of the NNW-SE Llobregat fault during the early Permian, explaining the high fracture density and the fast upflowing of hydrothermal fluids at that time, thus controlling the development of albite veins exclusively in this area.

1. Introduction

Fluids are ubiquitous in the Earth's crust and play a main role in diagenetic processes, metamorphism and the formation of ore deposits as they transport heat and dissolved ions (Fyfe et al., 1978; Ferry and Dipple, 1991; Deming, 1994; Garven, 1989; Duddy et al., 1994; Putnis, 2002; Trincal et al., 2015). A broad variety of fluid flow types occurs in the upper to middle crust, including flow along brittle faults and ductile shear zones, convection and pervasive fluid flow, which are driven by deformation and temperature gradients (Oliver, 1996, 2001). These fluid flow types cover a wide range of scales, from centimetric to regional scale (Oliver, 1996; Berwouts et al., 2008).

During shallow burial, fluids are produced by diagenetic reactions and by the expulsion of connate fluids during compaction, but external fluids may also enter in the system (Moore, 1989). As pressure and/or temperature increase, and prograde metamorphic conditions are achieved, fluids are produced by devolatilization reactions of hydrous minerals contained in metasedimentary sequences (Walther and Orville, 1982; Ferry and Dipple, 1991; Connolly, 1997, 2010). Afterwards, during uplift, external fluids (basinal and meteoric) infiltrate in the rocks producing the retrogression of the rocks and the generation of new veins under different P-T conditions (Fyfe et al., 1978; Zhang et al.,

* Corresponding author.
E-mail addresses: i_cantarero@ub.edu (I. Cantarero), galias@ub.edu (G. Alías), d.cruset@ub.edu (D. Cruset), eloicarola@gmail.com (E. Carola), pierre.lanari@geo.unibe.ch (P. Lanari), atrave@ub.edu (A. Travé).

https://doi.org/10.1016/j.gloplacha.2018.03.002
Received 31 May 2017; Received in revised form 23 February 2018; Accepted 6 March 2018
Available online 16 March 2018

2003; Anderson et al., 2004). Thus, during deformation and basin evolution, fluids evolve and change in terms of: 1) their hydrogeologic regime (open or closed) (Marquer and Burkhard, 1992; Travé et al., 1998; Ghisetti et al., 2001; Cruset et al., 2016); and, 2) their chemistry and composition due to e.g. fluid interaction with different lithologies, temperature and pressure changes that control the solubility/precipitation and stability barriers of minerals, redox reactions, fluid mixing caused by changes in the hydrogeologic regime and/or deformation, etc. (Barnaby and Rimstidt, 1989; Hanor, 1994; Labaume and Moretti, 2001; Parcerisa et al., 2006; Baqués et al., 2012; Lacroix et al., 2012).

On the other hand, fluid generation may increase the fluid pressure, which causes a decrease in the effective normal stress favoring failure and even induce the reactivation of misoriented faults at a given stress field (Sibson, 1977; Sibson and Scott, 1998; Aydin, 2000; Van Noten et al., 2011). Moreover, as fluids control the effective strength of rocks, they also exert a control in the transition zone between brittle and ductile conditions together with the geothermal gradient, lithology and grain size, inherited fabrics and stress field orientation (Connolly, 1997; Imber et al., 2001). Thus, fluids and deformation have an intrinsic relationship as fluids enable deformation and deformation facilitates fluid migration.

The study of veins, the best evidence of fluid flow, from a structural, petrological and geochemical point of view, provides insight about the relationship among deformation, metamorphism and fluid flow (Dewaele et al., 2004; Miller and Cartwright, 2006; Berwouts et al., 2008; Van Noten et al., 2008; Pitcairn et al., 2010; Depoorter et al., 2014). Quartz veins are present in most of exhumed metamorphic rocks and are generally believed to represent active fluid paths during or slightly after deformation and metamorphism, thus registering the P-T path and fluid chemistry during and after metamorphism (Nesbitt and Muehlenbachs, 1989; Wood and Walther, 1986; Yardley, 1986; Ferry and Dipple, 1991; Birtel and Stöckhert, 2008; Berwouts et al., 2008).

This work deals with the temporal and spatial relationship between fluids and deformation in an isolated horst of the Catalan Coastal Ranges (NE Iberia), mainly constituted of Ordovician phyllites. This horst, the Turó de les Forques, is differentiated from the surrounding areas by a complex network of fractures including syn- to late-cleavage Hercynian veins and faults and veins generated during different extensional and compressional events registered in the Catalan Coastal Ranges. The relationships between deformation and fluid flow in the Mesozoic and Cenozoic tectonic events have been previously studied in Mesozoic and Neogene carbonates (Travé et al., 1998; Baqués et al., 2010, 2012) and also in Neogene siliciclastic rocks (Travé and Calvet, 2001; Travé et al., 2009; Parcerisa et al., 2005; Cantarero et al., 2014a). For the first time, in this work, the study of such relationships is focused in the metamorphic Paleozoic basement in order to decipher the behavior of a crystalline basement with respect to fluids from Hercynian to Neogene times.

The aims of this study are fourfold: (i) to characterize petrologically and geochemically the mineral paragenesis related to the different generations of fractures; (ii) to determine the composition and origin of fluids; (iii) to establish the hydrogeological regimes and the fluid pathways as a function of the involved tectonic event; and (iv) to decipher the structural evolution of this isolated horst and why it concentrates that high density of fractures.

2. Geological setting

The Catalan Coastal Ranges (CCR), located in NE Spain, are the result of a long tectonic history that spans from Paleozoic to Present times. Nowadays, the CCR display a well-developed NE-SW horst-and-graben structure acquired during the opening of the Valencia Trough (Oligocene-early Miocene) (Roca and Guimerà, 1992). This structure is limited by NE-SW striking listric normal faults (Fig. 1), with a detachment level at 12–16 km (Gaspar-Escribano et al., 2004), segmented by later NW-SE to NNW-SSE trending faults. This Neogene extensional structure is superimposed on a Paleogene contractional structure, the Catalan Intraplate Chain, formed during the N-S collision between the Iberian and European plates during Late Cretaceous-late Oligocene (Guimerà, 1984; Bartrina et al., 1992). In its turn, NE-SW Paleogene thrusts were the result of the inversion of major Mesozoic normal faults (Guimerà, 1984; Bartrina et al., 1992; Roca, 1994; Vergés and García-Senz, 2001) that resulted from the western Tethys and of the North Atlantic openings. Moreover, previously to these tectonic events, Hercynian deformation and late-Hercynian processes also took place as recorded by the outcropping Paleozoic rocks within the horsts (Julivert and Duran, 1990a, b; Santanach et al., 2011; Cantarero et al., 2012, 2014b). In general, three Hercynian deformation phases have been reported: a main deformation phase responsible of the E-W trending folds and a main regional foliation and two late folding phases that formed crenulations to chevron and kink folds and related cleavages (Julivert and Duran, 1990a). After these folding phases, but before Triassic, late-Hercynian acidic to intermediate plutonic and hypabyssal rocks intruded the Cambro-Ordovician to Lower Carboniferous metamorphic sequence (Enrique, 1990). On a larger scale, this orogeny generated the curved Ibero-Armorican belt caused by the oblique convergence and collision of Gondwana and Laurentia-Baltica supercontinents at the end of the Paleozoic (Matte, 2001). The CCR belong to the northern limb of this arc where mainly greenschist facies conditions were acquired (Julivert and Duran, 1990b).

The Turó de les Forques is a horst, constituted by Ordovician phyllites, isolated within the Miocene rocks of the Vallès Half-graben, which is separated to the west from the Garraf Massif by the incision of the Llobregat River (Fig. 1). These rocks are unconformably overlain to the north by Miocene rocks, gently dipping to the NW, and are limited to the E by NNW-SSE and NE-SW striking normal faults dipping to the E-SE. At the other side of the Llobregat river, Ordovician phyllites are unconformably overlain by Buntsandstein facies (Fig. 1). Both Buntsandstein and Miocene successions are only gently tilted (10–20°), indicating the scarce rotation of the rocks forming the Turó de les Forques.

The incision of the Llobregat River has exposed a 500 m long and 80 m high excellent outcrop, intensely crosscut by a huge amount of fractures resulting from a complex tectonic history from Hercynian to Neogene times.

3. Methodology

The field work carried out in this study allowed to generate a schematic map and a cross-section of the Turó de les Forques (Fig. 2). Structural data was collected and plotted in equal-area lower-hemisphere stereographic projections (Fig. 3). The remarkable outcrop parallel to the highway was mapped and the different fractures sets and their crosscutting relationships were established (Fig. 3). The different generations of fractures, fault rocks and vein minerals, were sampled. Thin sections were studied under optical and cathodoluminescence microscopes. A Technosyn Cold Cathodoluminescence Model 8200 MkII operating at 16–19 kV and 350 μA gun current was used.

X-ray diffractions of 7 whole-rock powders have been performed with a Bragg-Brentano PAnalytical X'Pert PRO MPD alpha 1 operating at 1.5406 Å, 45 kV and 40 mA. They were scanned from 4 to 100°2θ with a 0.017°2θ step size and a count time of 50 s per step. Oriented aggregates of clay minerals in gouges were also prepared in order to recognize the mineralogy. Samples were dispersed and disaggregated by soaking in de-ionized water and suspended repeatedly. Separation of the < 2 μm fraction was done by centrifugation. Samples were subsequently air-dried, glycolated during 24 hours at 50 °C and heated for 2h at 550 °C. XRD patterns were obtained between 2 to 62°2θ (normal sample) and 2 to 30°2θ (ethylene glycol and thermal treatment samples) with a 0.033°2θ step size and a count time of 50 s per step.

Ordovician phyllites and gouges have also been analyzed by X-Ray

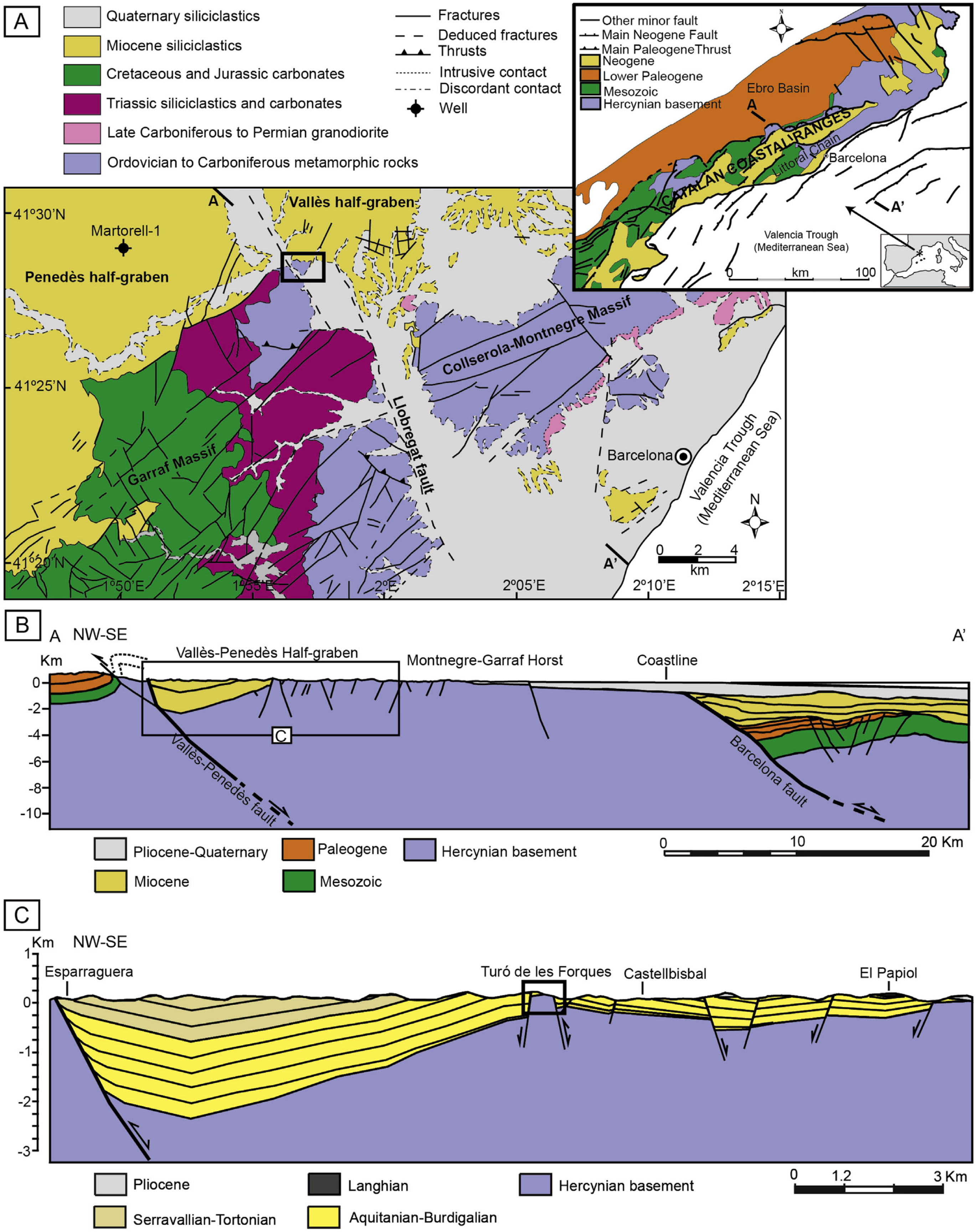

Fig. 1. Geological setting. A) Location and schematic map of the Catalan Coastal Ranges and magnification of the Littoral Chain around the study area. The black square indicates the location of the Turó de les Forques. The location of the well Martorell-1 is indicated. B) Cross-section of the CCR indicated in the inset of A (from Travé et al., 2009). C) Enlargement of the squared area in the cross-section shown in B. The square marks the location of the Turó de les Forques study area (Fig. 2).

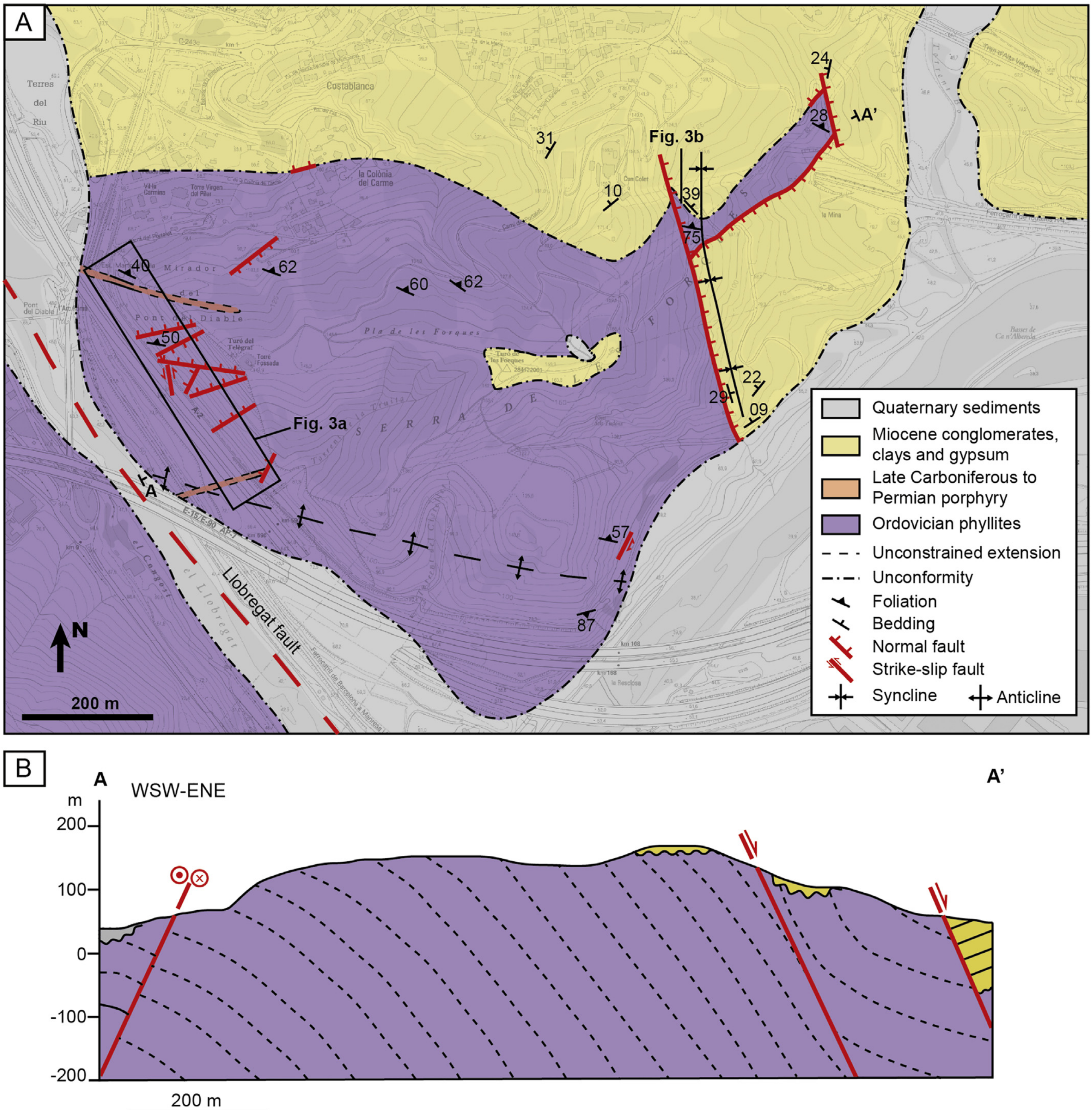

Fig. 2. A) Geological map and B) cross-section of the Turó de les Forques. Location of Fig. 3 is indicated.

Fluorescence (FRX). Major elements were measured in fussed samples with a Panalytical PW 2400 spectrophotometer, using an Rh anode. Fussed samples were prepared with 0.3 g of molten and dry sample mixed with 5.7 g of lithium tetraborate and 5 mg of lithium iodide. The mixture was homogenized and fussed at 1125 °C obtaining pearls of 30 mm of diameter.

Carbon-coated thin sections were used to analyse major and minor elements of carbonate cements, chlorites, feldspars and micas with a CAMECA SX-50 electron probe micro-analyzer (EPMA). It was operated using 15 nA beam intensity, 20 keV acceleration voltage and a beam diameter of 10 µm. The precision of major elements is about 0.64% (at 2σ confidence level).

Twelve microsamples of calcite cements were powdered with a microdrill for carbon and oxygen isotopes. Samples (60 ± 10 µg) were reacted with 100% phosphoric acid at 70° C for three minutes. The CO_2 extraction was done in an automated Kiel Carbonate Device III attached to a Thermal Ionization Mass Spectrometer Thermo Electron (Finnigan) MAT-252 following the method of McCrea (1950). The International Standard NBS-19 was used. The results are expressed in ‰ VPDB standard. Standard deviation is ± 0.02‰ for $\delta^{13}C$ and ± 0.07‰ for $\delta^{18}O$.

Temperature conditions were estimated both, by thermometry from chlorite composition and by fluid inclusion analyses.

Chlorite present several chemical substitutions (simple and coupled) controlled by the equilibrium conditions (P, T, pH, fO_2) that can be modeled using a set of different end-members (Vidal et al., 2001, 2005, 2006, 2016; Lanari et al., 2014). In this work the multi-equilibrium approach of Vidal et al. (2005, 2006) was used to obtain the simultaneous estimate of Fe^{3+} content in chlorite and equilibrium temperature by the convergence of four equilibria reactions involving five chlorite end-members (Mg-amesite ($Si_2Al_4Mg_4O_{10}(OH)_8$), Fe-amesite ($Si_2Al_4Fe_4O_{10}(OH)_8$), daphnite ($Si_3Al_2Fe_5O_{10}(OH)_8$), clinochlore ($Si_3Al_2Mg_5O_{10}(OH)_8$), and sudoite ($Si_3Al_4Mg_2\square_1O_{10}(OH)_8$)) at a given pressure (Vidal et al., 2005). The position of these equilibria in a P-T space depends on the activities of the chlorite end-members, quartz and water (Berman, 1991). In this work, temperatures and XFe^{3+} of chlorite were estimated at a fixed pressure of 2 kbar, taking into account that Hercynian metamorphism is LP-HT and that a pressure of 1.5 kbar has been reported for the late-Hercynian granodiorite intruding the Ordovician host rocks in a nearby area at the Littoral Chain (Gil Ibarguchi and Julivert, 1988). Water activity has been considered equal to 1. The convergence is achieved for a minimum Fe^{3+} fraction ($XFe^{3+} = Fe^{3+}/(Fe^{2+}+Fe^{3+})$) when the temperature difference between the four equilibria is less than 30 °C (Lanari et al., 2012 and references therein). Formation temperatures of chlorite in the current study were estimated using the program ChlMicaEqui (Lanari, 2012).

Fluid inclusions were examined in quartz and calcite to determine composition and temperature of the mineral-forming fluid. Thick sections were used for petrographic characterization of the fluid inclusions and for microthermometric determination. Measurements were made on a Linkam THM-600 heating-freezing stage. Raman microspectroscopy analyses were recorded with a LabRam HR800 Jobin-Yvon™ microspectrometer equipped with 600 g/mm gratings and using 532 nm (green) laser excitations. Acquisition timespan was 30 s and 60 s during 10 accumulation spectra. Vapor bubbles were analyzed in order to determine the presence of volatile species (CO_2, CH_4, N_2, H_2S). Due to fluorescence interferences, fluid inclusions only have been analyzed in quartz 1.

4. Structure

The Ordovician phyllites show a regional foliation that dips dominantly 60° to the NNE which is deformed by km-spaced WNW-ESE open folds (Fig. 2, 3). The foliation corresponds to a penetrative cleavage which is locally deformed in centimetric kink folds with axial planes dipping around 80°E. These orientations are consistent with the Hercynian structures described at regional scale (Julivert and Duran, 1990a). The phyllites are intruded by two granodioritic porphyries of NE-SW direction.

Based on field and thin section cross-cutting relationships, orientation, geometry and vein mineralogy, 9 fracture types have been described, being from the oldest to youngest: syn-cleavage quartz veins, late-cleavage quartz veins, en-echelon albite veins, NE-SW normal faults, NE-SW dolomite veins, NW-SE reverse faults, N-S calcite veins, NE-SW Neogene normal faults and NNW-SSE Neogene normal faults. The first seven generations have only been found in the Ordovician phyllites whereas the last two fault systems affect both Ordovician phyllites and Miocene rocks.

Syn-cleavage quartz veins. Veins are from 1 to 50 cm wide and are concentrated into 4-meter thick bands separated by a metric spacing. Veins occur in moderate to tight rounded folds with axial-planes parallel to cleavage. In the limbs the veins are dismembered parallel to the cleavage, whereas in the hinge, veins are thickened (Fig. 3, 4A). These observations point out that these veins are coeval to the development of the Hercynian cleavage.

Late-cleavage quartz veins. These veins cross-cut the previous quartz veins and are less abundant. They are 1 to 7 cm wide and up to 1 m long and are developed perpendicular to the cleavage (Fig. 3, 4B). However, locally, they are slightly deformed by open folds, which axial plane is the regional cleavage. That relationship suggests that these veins were formed during the last stages of the cleavage development. Moreover, at microscopic scale, these veins are affected by discontinuous ductile shears, about 2 cm long and 200–500 μm wide, subparallel to the vein walls, thus confirming the Hercynian age of these veins.

En-echelon albite veins. Veins have a N-S to NE-SW striking direction with a steep dip towards the W (Fig. 3). Veins are from 3 to 15 cm long and from 1.5 mm to 5 cm wide and have both straight and sigmoidal shapes (Fig. 4C, D). They have a characteristic pinkish color due to the albite. The thickest veins usually contain angular phyllite clasts (Fig. 4E). Also the coalescence of several veins produced a brecciation of the rock. These veins are not homogeneously distributed along the outcrop. They are disseminated in the host rock with densities from 11 to 75 fractures/m or are arranged in en-echelon vein arrays (Fig. 3, 4). Such arrays are both single and conjugate sets with a mirrored symmetry and indicate a normal displacement. In some cases, these arrays are linked to discrete fault planes (Fig. 4D).

NE-SW normal faults. Faults are normal and transtensional with a dominant NE-SW trend and dips between 63 and 87° indistinctly to the NW or SE, in a conjugate system. Plains are usually undulouse, producing variations in the strike direction (Fig. 3). These faults generate breccias constituted by angular clasts derived from the phyllites, up to 3 cm in size, and from albite veins, which are in turn cemented by albite. This fact suggests successive fault movements and albite precipitation. Locally these faults have been reactivated as strike-slip. This reactivation generates greenish cohesive cataclasites constituted by millimetric to centimetric clasts from the host rock and albite veins (Fig. 4F).

NE-SW dolomite veins. These veins, up to 400 μm wide and up to 3 cm long, have only been recognized at microscopic scale. They show a NE-SW trend with dips between 35–45°SE.

NW-SE reverse faults. This set of fractures are poorly developed and represents reverse faults defined by NW-SE discrete planes dipping around 35° to the NE (Fig. 3).

N-S calcite veins. These veins, up to 2 mm wide, have been only recognized at microscopic scale. They show a N-S striking direction and are subhorizontal.

NE-SW Neogene normal faults. This system affects both the Ordovician phyllites and the Miocene rocks, thus indicating their Neogene age. They are represented by NE-SW normal faults with dips from 25 to 80 mostly to the NW (Fig. 3). This dip variability is caused by the characteristic fan-like geometries of this system (Fig. 3). These geometries are formed by both discrete planes or up to 1.5 m wide fault cores, only in the phyllites, defined by greyish fault gouges (Fig. 4G).

NNW-SSE Neogene normal faults. These faults cut and displace the Miocene unconformity and the Miocene rocks above, indicating their formation during the Neogene extension (Fig. 3B).This fault system is defined by a conjugate system of NNW-SSE trending normal faults dipping 52–79° indistinctly to the W or E, later reactivated as strike-slip faults (Fig. 3B-C). These faults are represented by discrete planes that locally develop centimetric fan-like geometries. This system commonly has striated planes, which are sometimes formed by calcite slickenlines (Fig. 3B).

5. The host rocks

Phyllites are characterized by a penetrative cleavage defined by a strong preferred orientation of chlorite, muscovite and elongated quartz with some interbedded quartz-rich layers, from 0.1 to 1.8 mm thick (Fig. 5A-C). Bedding shows syn-cleavage tight folds with thickened hinges, with axial planes and limbs parallel to the regional foliation (Fig. 5B). This foliation is locally folded by minor crenulations (Fig. 5D) and kink folds.

Pelitic bands are constituted by muscovite (60%), quartz (25%), chlorite (10%) and albite (5%) and are rich in organic matter. Muscovite crystals range in size from 0.01 to 0.05 mm, quartz and albite from 0.02 to 0.1 mm and chlorite from 0.05 to 0.15 mm. On the other hand, quartz-rich layers have a granoblastic texture constituted by quartz (60%), muscovite (35%) and chlorite (5%). Quartz has a grain size between 0.05 and 0.1 mm, muscovite between 0.02 and 0.15

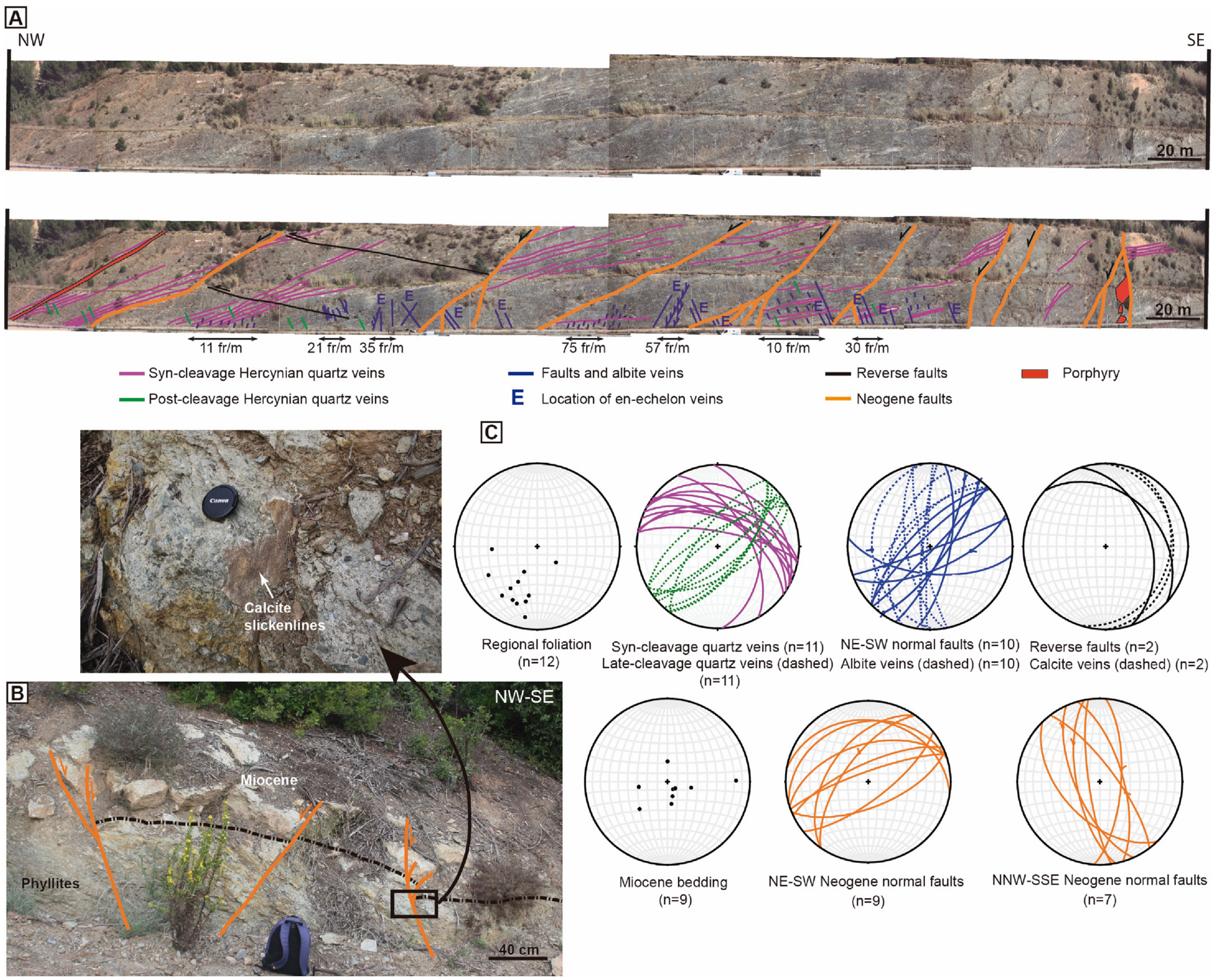

Fig. 3. A) View of the main outcrop formed by the Ordovician phyllites representing the distribution and orientation of the different fracture systems. Some of the structures could only be drawn in the lower half of the outcrop due to the impossibility of access to the upper outcrop section in order to check their distribution. B) Unconformity between Ordovician phyllites and Miocene rocks displaced by NNW-SSE normal faults and detail of the calcite slickenlines in the fault plane crosscutting the unconformity. C) Lower-hemisphere equal-area stereoplots of Miocene bedding, regional foliation and the different sets of faults and veins.

mm and chlorite between 0.1 and 0.2 mm. Quartz and chlorite are elongated parallel to the regional foliation and show intracrystalline deformation, indicating a pre-foliation development (Fig. 5A, C), whereas the preferred orientation of prismatic muscovite crystals (Fig. 5C), points to a syntectonic crystallization.

Miocene rocks from the Costablanca Formation (Burdigalian; Anadón and Cabrera, 1980; Cabrera, 1981), unconformably overlying the Ordovician phyllites, consist of an alternance of lacustrine carbonates, red conglomerates and white to red lutitic layers. Lacustrine carbonates are mudstones with levels rich in filamentous microbial-like structures and a dull orange cathodoluminescence.

Miocene limestones show $\delta^{18}O$ values between −8.6 and −8 ‰VPDB and $\delta^{13}C$ values between −7.7 and −6.5 ‰VPDB (Fig. 6).

6. Paragenetic sequence in fractures

The 9 different fracture types described above are characterized by different mineral associations, leading to the following paragenetic sequence (Fig. 7):

6.1. Quartz 1-chlorite 1 ± muscovite

This mineral association constitutes the main paragenesis of the syn-cleavage and late-cleavage quartz veins. In both types of veins, quartz 1 crystals are inequigranular, up to 7 mm in size, inclusion-rich and have undulouse extinction (Fig. 8A). Quartz crystals in syn-cleavage veins show intracrystalline deformation and partial recrystallization represented by subgrain formation, deformation lamellae and lobate grain boundaries (Fig. 8A). This intracrystalline deformation is less intense in late-cleavage quartz veins, which crystals are elongated and bladed and grain boundaries are straight or curved.

Chlorite 1 grows along the contact between quartz crystals. It is characterized by brownish crystals up to 62 μm in size. Though less abundant, muscovite flakes up to 200 μm are associated with chlorite (Fig. 8B). Chlorite and muscovite of the host rock form larger crystals, up to 350 μm, along the contact with the quartz-vein probably due to host rock recrystallization during vein formation (Fig. 8C).

6.2. Quartz 2-chlorite 2-dolomite 1

This mineral association is related to discontinuous ductile

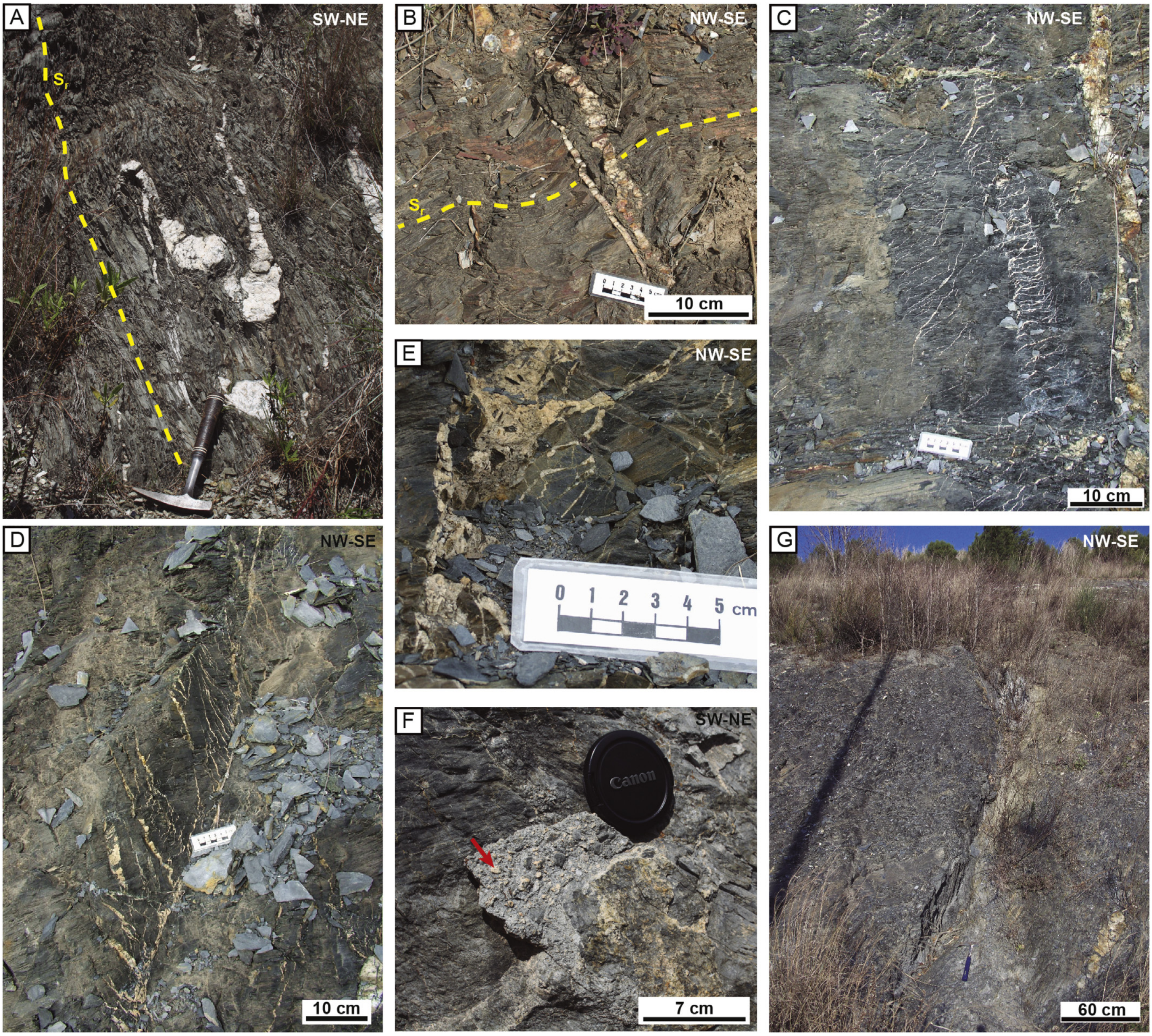

Fig. 4. Field images of fractures. A) Syn-cleavage folded quartz vein. The dashed line defines the regional foliation (S_r), which defines the axial plane of the fold. B) Late-cleavage quartz vein. C) Two single en-echelon albite vein arrays, formed by sigmoidal veins. D) En-echelon albite vein array, formed by straight veins, associated to two discrete fault planes. E) Phyllite breccia cemented by albite. F) Cataclasite associated to the strike-slip reactivation of a NE-SW normal fault. Clasts made of albite cement are highlighted by their pinkish color (red arrow). G) NE-SW Neogene normal fault with a thick fault core formed by a grey gouge. (For interpretation of the references to color in this figure legend, the reader is referred to the web version of this article.)

microshears and microveins developed in the late-cleavage quartz veins (Fig. 8D-E). This late stretching also caused the elongation of quartz crystals, perpendicularly to the veins, with this mineral association precipitating in the triple points between the elongated quartz crystals (Fig. 8F).

Quartz 2 crystals have less inclusions than the previous quartz generation and grow in optical continuity with the hosting quartz 1 crystals. Dolomite 1 cement is characterized by rhombic and subhedral crystals, 60 μm and 50 to 100 μm in size, respectively. Chlorite 2 is characterized by vermicular morphologies, from 53 to 174 μm long and from 15 to 50 μm wide, and it is included within the quartz 2 crystals and dolomite 1 crystals (Fig. 8E-F).

6.3. Albite-quartz 3-chlorite 3 ± titanite-anatase

This paragenesis is found in en-echelon albite veins and breccias formed in the NE-SW normal faults. A temporal evolution is observed in these veins:

The first veins, up to 1.5 mm wide, are characterized by the presence of elongated to euhedral albite and quartz (Fig. 9A). These incipient veins are crosscut by straight and sigmoidal veins mainly formed by albite. These types of veins postdate the minor crenulations formed during the late Hercynian folding phases (Fig. 9B). During and after late veining, breccias were also formed (Fig. 9C). In this deformation, albite is characterized by prismatic crystals, from 50 to 770 μm in size, with Carlsbad twinning. The albite has a composition above 95% albite, as shown by EPMA, and it is usually altered to kaolinite. Quartz 3 is inclusion-free, and forms 150–400 μm in size

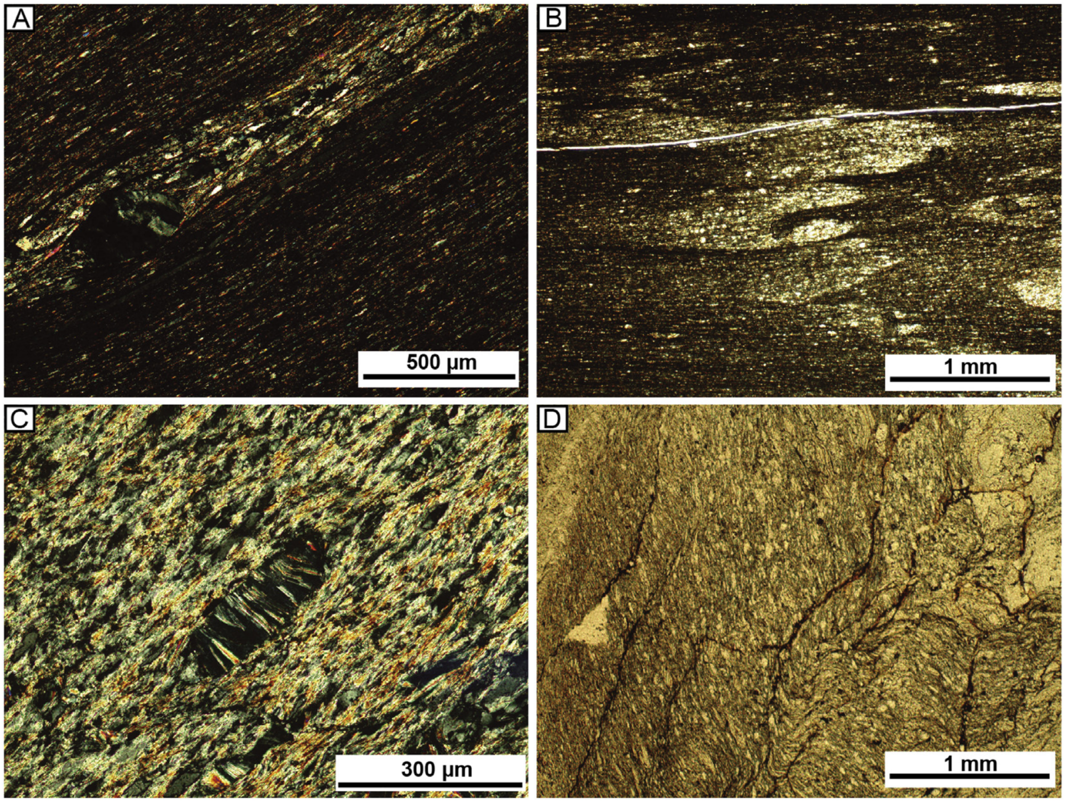

Fig. 5. Microphotographs of the Ordovician phyllites. A) Regional foliation parallel to the compositional pelitic and quartz-rich layers (cross polarized light, XPL). B) Syn-cleavage folding of the bedding, defined by quartz-rich layers (plane polarized light, PPL). C) Regional foliation defined by muscovite, chlorite and elongated quartz (XPL). D) Crenulation of the the regional foliation (PPL).

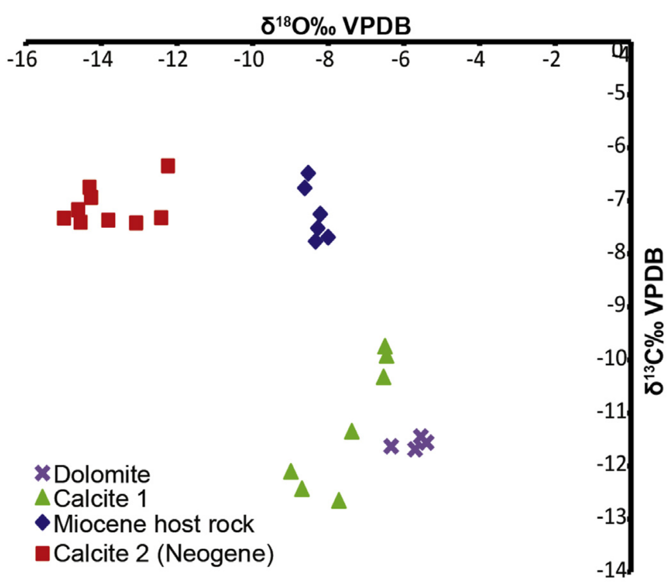

Fig. 6. $\delta^{18}O$ and $\delta^{13}C$ cross-plot of the host Miocene limestones, calcite and dolomite cements.

subhedral crystals. Chlorite 3 is characterized by 30–60 µm in size vermicular crystals included in the albite and quartz crystals and fibrous-radial aggregates, with 300 µm long fibers, between crystals and forming planes at vein walls (Fig. 9D-E). Titanite and anatase grains are occasionally found (Fig. 9F).

6.4. *Dolomite 2-chlorite 4-quartz 4*

This paragenesis is developed in the NE-SW dolomite veins and vugs affecting the quartz 1 crystals (Fig. 10) and postdates the albite-quartz3-chlorite3 ± titanite-anatase association (Fig. 10A). Vugs are up to 1 mm in diameter and have irregular borders (Fig. 10E-F). Quartz 4 is inclusion-free and grows in optical continuity with the hosting quartz crystals. Dolomite 2 is represented by dull red, 50 to 340 µm, subhedral crystals in fractures and 100 µm in size rhombs with a dull red to orange concentric zonation in vugs (Fig. 10B-F). Finally, chlorite 4 has vermicular morphologies associated to dolomite fractures and forms irregular masses in vugs (Fig. 10B-C, E).

Dolomite is characterized by $\delta^{18}O$ values between −6.3 and −5.4 ‰VPDB and $\delta^{13}C$ values between −11.7 and −11.4 ‰VPDB (Fig. 6).

6.5. *Calcite 1-barite*

This association is present in the N-S subhorizontal calcite veins and partially cementing the cataclasites produced during the strike-slip reactivation of NE-SW normal faults.

Calcite 1 is characterized by euhedral drusy, 40 µm to 1 mm in size, crystals with a zoned orange cathodoluminescence (Fig. 10D, 11A-B). Barite forms prismatic crystals, up to 1.5 mm long and 140 µm wide and, together with calcite 1, cements the cataclasites and microfractures in quartz 1 crystals (Fig. 11C-D).

The calcite 1 shows $\delta^{18}O$ values between −9 and −6.5 ‰VPDB and $\delta^{13}C$ values between −12.7 and −9.7 ‰VPDB (Fig. 6).

6.6. *Gouges*

Greyish fault gouges are formed in the NE-SW Neogene normal faults. They are constituted by quartz, muscovite, chlorite, albite and anatase resulting from the comminution of the phyllites and newly formed illite, smectite and kaolinite. Fault gouges change moderately the global bulk composition of the Ordovician phyllites, represented by

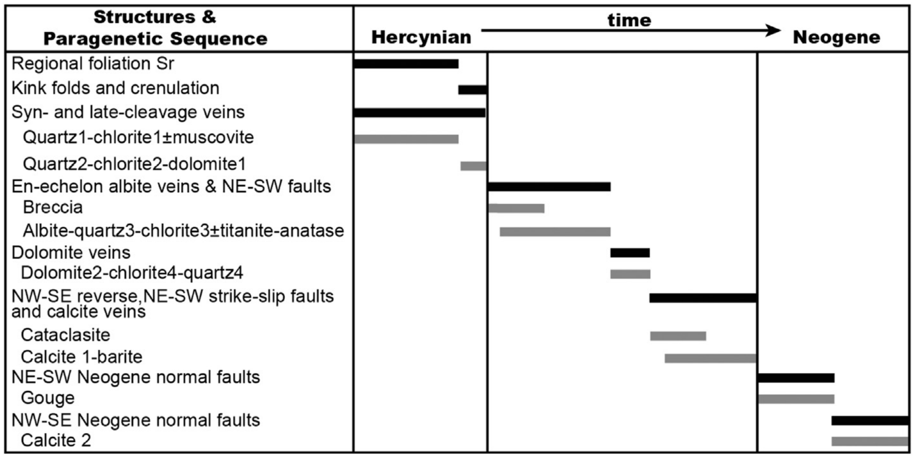

Fig. 7. Structures and paragenetic sequence of the Turó de les Forques. Black lines: structures; grey lines: faults rocks and mineral associations.

a decrease of the SiO_2 content together with an increase in Al_2O_3 and K_2O. This is consistent with an increase of white mica (illite formation) and loss of chlorite in the gouges respect to the host rock.

6.7. Calcite 2

Calcite 2 cement is present in the NNW-SSE Neogene fractures. It is characterized by subhedral crystals, from 80 to 520 μm in size, with orange luminescence and a drusy disposition in the main fault planes (Fig. 12A-B) and by subhedral to rounded crystals, from 60 μm to 1 mm in size, with orange to non-luminescent zonation and a blocky disposition in joints (Fig. 12C-D).

Calcite 2 cement has $\delta^{18}O$ values between −15 and −12.2 ‰VPDB and $\delta^{13}C$ values between −7.4 and −6.3 ‰VPDB (Fig. 6).

7. Thermometry

7.1. Chlorite chemistry and T-XFe^{3+} estimates

The chemical composition of chlorites in the phyllites (abbreviation: chl_0) and the four vein-filling paragenesis (chlorites 1 to 4, abbreviations: chl_1, chl_2, chl_3, chl_4) was determined by EPMA. Two main groups are distinguished based on variations in SiO_2, FeO, MgO and MnO contents. The first group is formed by the chlorite in the host rocks chl_0 and chlorites chl_1, chl_2 and chl_3. SiO_2 ranges between 24 and 28.6 wt.%, FeO between 20 and 36.8 wt.% (with mean values slightly lower in the phyllites), MgO between 4.9 and 19.6 wt.% and MnO between 0.1 and 1 wt.%. On the other hand, the second group formed by chl_4 exhibits higher SiO_2, MgO and MnO contents (26.7–29.6 wt.%, 13.4–19.3 wt.% and 0.3–2.9 wt.% respectively), and slightly lower FeO content (19.4–28.3 wt.%). Similar trends are observed in the structural formula composition expressed in atom per formula unit (apfu). Si content ranges between 2.6 and 2.8, Fe between 2.2 and 3.4, Mg between 0.8 and 2.3 and Mn between 0.015 and 0.1 in the $chl_{0\text{-}3}$ and, between 2.8-3 apfu, 1.6-2.5, 2.1-2.9 and 0.02-0.26, respectively, in chl_4 (Fig. 13). Thus, according to Foster (1962), $chl_{0\text{-}3}$ are dominantly classified as ripidolites and chl_4 as brunsvigites. However, Al_2O_3 ranges between 22.9 and 23.2 wt.% in Chl_0, 19–24.2 wt.% in $chl_{1\text{-}3}$, and 16.7–21.9 wt.% in chl_4. Major differences are produced in the Al^{VI} position with: 1.5–1.7 (chl_0), 1.2–1.6 ($chl_{1\text{-}3}$) and 1.1–1.4 (chl_4) whereas Al^{IV} is 1.1–1.4 ($chl_{0\text{-}3}$) and 1–1.2 (chl_4).

Crystallization temperature and XFe^{3+} of chlorite were estimated using the calibration of Vidal et al. (2005, 2006). Convergence was not achieved in the P-T-XFe^{3+} space for the chl_0 composition observed in the phyllites. Chl_1, chl_2 and chl_3 are characterized by low XFe^{3+} values of 0.07–0.33 (0.14 in average) and temperatures ranging between 237 and 343 °C (290 °C in average) (Fig. 13). By contrast, chl_4 are characterized by higher XFe^{3+} of 0.46 ± 0.06 and slightly lower temperatures, ranging between 234 and 309 °C (261 °C in average) (Fig. 13).

7.2. Fluid inclusions

Fluid inclusions analyses have been performed in quartz and calcite veins.

The petrographic analysis revealed that quartz 1 (qtz_1-chl_1-mu), quartz 3 (qtz_3-ab-chl_3) and quartz 4 (qtz_4-chl_4-dol_2) are characterized by small (2–10 μm) primary aqueous biphase liquid-rich fluid inclusions (25% vol. gas bubble), suitable for microthermometry measurements. On the other hand, in calcite 1 and 2, primary monophase aqueous fluid inclusions, between 2 and 12 μm in size, observed in growth zones of calcite crystals remained monophasic after cooling for 7 days at 4 °C.

Fluid inclusions in quartz 1 show homogenization temperatures between 230 and 370 °C (with most values between 240 and 320 °C), quartz 3 between 140 and 310 °C (180–270 °C) and quartz 4 between 157 and 330 °C (180–300 °C) (Fig. 14). Thus, the four quartz generations show very similar range of temperatures, with a slight temperature decrease in quartz 3 and 4. The pattern and the absolute values are both in line with the results obtained by chlorite thermometry.

In all the quartz generations, melting temperatures above 0 °C were obtained, indicating the presence of clathrates. Salinities, for the negative T_m values, were calculated in the binary H_2O–NaCl system, using the equation of Bodnar (1993). In quartz 1, T_m ranges between −6 and +8 °C (Fig. 14), obtaining salinity values between 0 and 7 wt% NaCl eq. Quartz 3 T_m ranges between −9 and +3 °C, indicating salinities between 7.8 and 12.8 wt% NaCl eq. Finally, quartz 4 has the highest T_m variability, between −21 and +9 °C (Fig. 14), indicating salinities between 0 and 23 wt% NaCl eq. The highest salinities, 20–23 wt% NaCl eq., are related to the lowest T_h ranging between 157–232 °C.

Raman analyses in fluid inclusions of quartz 1 showed the presence of 0–3% CH_4 and 0–41% N_2 in addition to 57–100% CO_2.

8. Discussion

8.1. Evolution from ductile to brittle deformation and related fluid

The association quartz-chlorite-muscovite-albite of the Ordovician phyllites of the Turó de les Forques indicate their formation during greenschist facies. The absence of biotite suggests that they formed at temperatures *ca.* 400 °C. The absence of intersection between the chlorite-quartz-water equilibria in the P-T-XFe^{3+} space for chl_0 could suggest formation temperature higher than 380 °C at low pressure (Lanari, 2012).

Syn-cleavage and late-cleavage quartz veins are highly frequent in

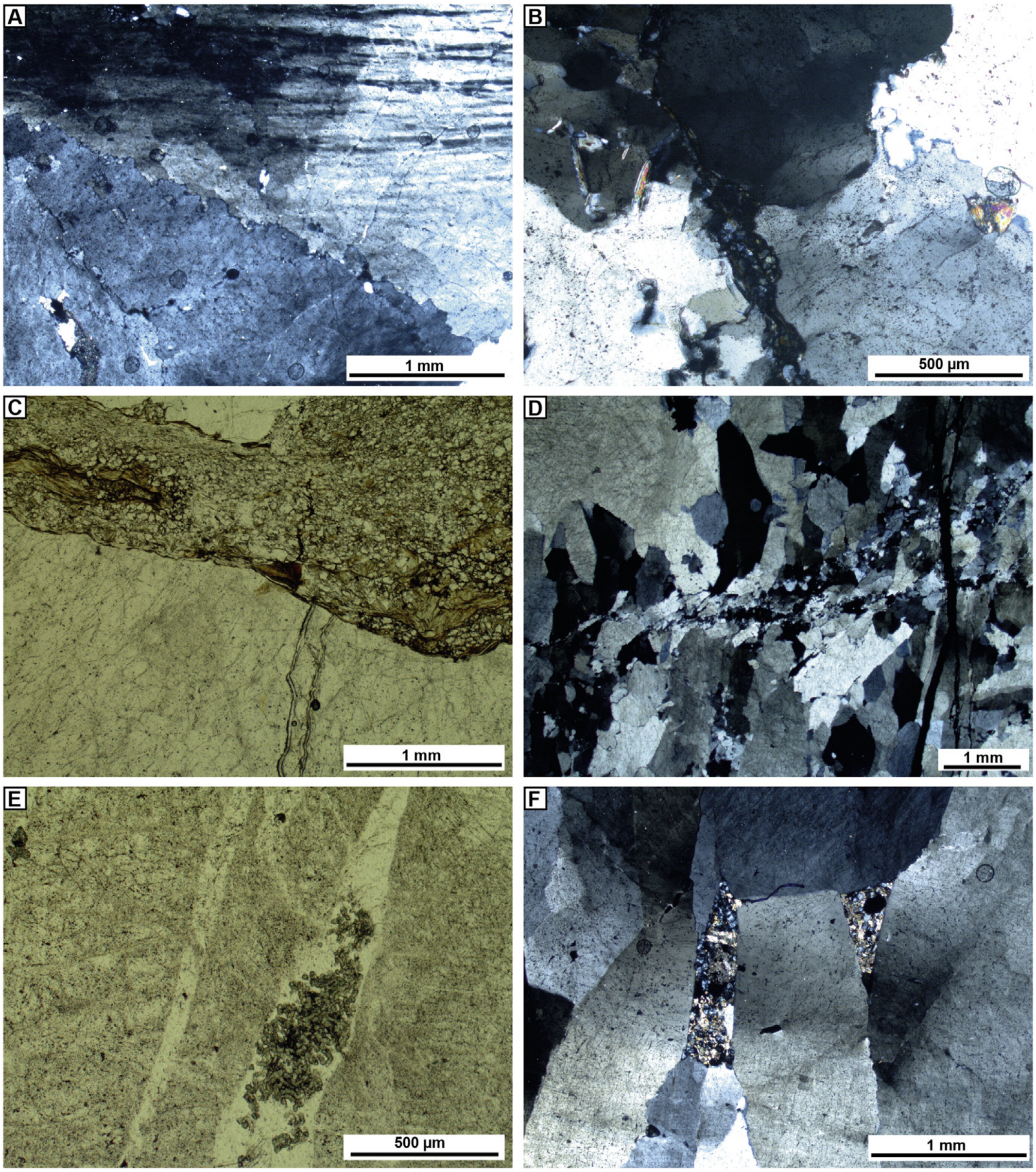

Fig. 8. Microphotographs of *syn*-cleavage and late-cleavage quartz veins. A) Quartz 1 crystals with undulouse extinction, subgrains, lobated grain boundaries and deformation lamellae (XPL). B) Chlorite 1-muscovite vein emplaced along quartz 1 crystals boundaries (XPL). C) Recrystallization of host rock chlorites along the border with the quartz 1 vein (PPL). D) Microshear, producing grain size reduction and recrystallization, associated with quartz elongation (XPL). E) Microvein formed by clear quartz and vermicular chlorites (PPL). F) Triple points, formed between elongated quartz crystals, and cemented with dolomite 1-chlorite 2-quartz 2 association (XPL).

Paleozoic low-grade metamorphic rocks along the CCR, as occurs in most metamorphic rocks, as they are inherently related to deformation and Si-rich fluids derived from metamorphism (Birtel and Stöckhert, 2008). The presence of carbonate in the metapelites, as pointed by Gil Ibarguchi and Julivert (1988), could be the source for dolomite 1. Also, the presence of the CO_2-N_2-CH_4 mixture in fluid inclusions is compatible with metamorphic fluids produced by devolatilization reactions and fluid-rock interaction in sedimentary sequences rich in organic matter under low-grade metamorphic conditions (Shepherd et al., 1991; Dee and Roberts, 1993; Yardley, 1997; Van Den Kerkhof and Thiéry, 2001; Kenis et al., 2005). Their related mineral paragenesis, chl_1-qtz_1-mu and chl_2-qtz_2-dol_1, show slightly lower temperature conditions than the host rock, 240–340 °C, as suggested by both fluid inclusions and chlorite thermometry. This result suggests that the veins formed at slightly lower temperatures than the ones achieved during the metamorphic peak.

It has been suggested that metamorphic fluids are the result of the continuous evolution of sedimentary pore fluids that are modified during diagenesis and metamorphism by devolatilization reactions as fluids interact with the host rocks at different P-T conditions (Yardley, 1997; Yardley and Graham, 2002). The protolith of the Ordovician phyllites consist of greywackes and shales deposited in deep-sea turbiditic sequences of a passive margin (Vilà and Pin, 2016). Salinities obtained from fluid inclusions in quartz 1 are similar to those of seawater (3.5 wt% NaCl eq.), suggesting that the metamorphic fluid has evolved from a marine connate fluid. Small salinity variations from this value can result from the addition of Cl due to Cl-OH and Cl-F exchange reactions between the fluid and hydrous minerals (salinity increase) and dehydration reactions produced during burial and prograde metamorphism (salinity decrease) (Smith and Yardley, 1999a, 1999b; Yardley and Graham, 2002; Vidal and Dubacq, 2009).

At mesoscale, quartz veins evidence fluid flow along fractures. Dehydration metamorphic reactions supply large volumes of silica-rich fluids during cleavage development that favours the formation of syn-

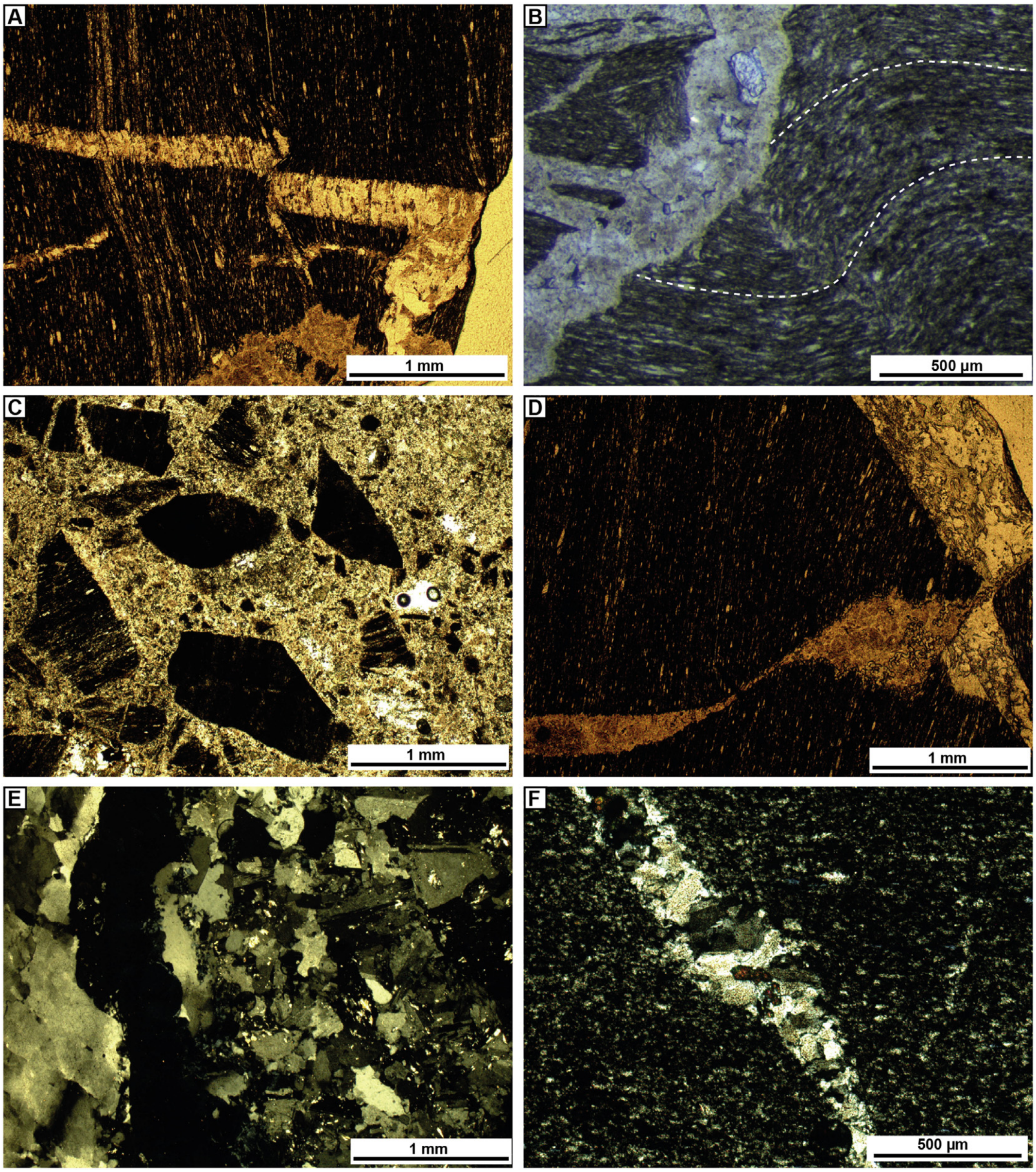

Fig. 9. Microphotographs of albite-quartz 3-chlorite 3 ± titanite-anatase paragenesis. A) Vein formed by elongated quartz and minor elongated albite (PPL). B) Vein of albite cross-cutting minor crenulations (PPL). C) Breccia cemented by the paragenesis albite-quartz 3-chlorite 3 ± titanite-anatase (PPL). D) Quartz 1-chlorite 1 vein displaced by an albite-chlorite 3 vein. Note the vermicular morphology of chlorites contained in the kaolinitized albite (PPL). E) Fibrous-radial chlorite aggregates at the contact between the quartz 1 vein (left) and albite-quartz 3-chlorite 3 vein (right) (XPL). F) Albite vein containing several anatase crystals (XPL).

cleavage veins formation. During the last stages of cleavage development, the remaining volume of silica-rich fluids is lower as observed with the minor development of late-cleavage veins. We interpret that this late cleavage-perpendicular fracturing was triggered by the decrease in overburden pressure caused by the denudation of the orogen, which produced a relative fluid pressure increase in a ductile regime. On the other hand at microscale, fluid flow also occurred along microshears and intercrystalline boundaries and precipitated in low-pressure areas such as triple points created between elongated quartz crystals (Fig. 15). Such a fluid flow, through interconnected grain boundaries and triple points, was favored by the temperature conditions. Below 300 °C and low pressures, the cooling contraction of quartz together with its extremely low diffusion and the stop of grain boundary migration generated the opening of grain boundaries (Kruhl et al., 2013). Thus, during metamorphism a coupled fluid flow system acted: a regional channelized fluid flow system giving rise to the mesoscopic quartz veins and a centimetric scale pervasive flow through grain boundaries and triple points.

After the development of quartz veins, the formation of albite veins and albite-cemented breccias in the NE-SW normal faults suggests a progressive change in the fluid composition indicated by the change from quartz-enriched to albite-dominated paragenesis. As no ductile deformation structures neither recrystallization textures have been observed related to albite veins, a brittle regime is interpreted in the formation of these veins. Therefore, the compositional variation of the fluids, from silica-rich to albite-rich, occurred during the transition from ductile to brittle conditions (Fig. 16). Moreover, the shear sense of the en-echelon vein arrays and the NE-SW normal faults indicate their formation during an extensional stress regime. At regional scale, two different deformation phases could cause the extensional structures: the early Permian extension and the late Permian-Early Jurassic rifting. The former, resulting from the collapse of the Hercynian orogen and associated with magmatism and the development of grabens filled with Permian deposits, has been observed in the Pyrenees and other

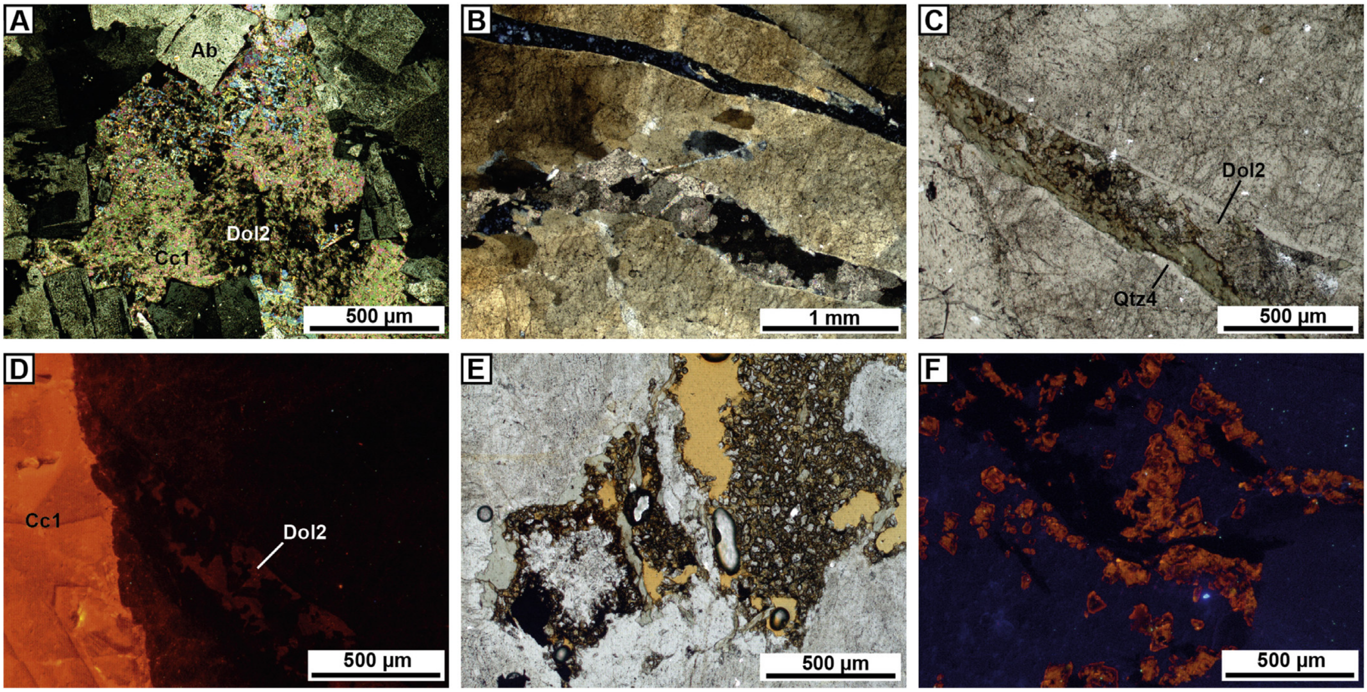

Fig. 10. Microphotographs of the dolomite 2-chlorite 4-quartz 4 paragenesis. A) Dolomite 2, partially calcitized by calcite 1, filling the remaining porosity after albite precipitation in a fracture (XPL). B) Dolomite 2 and chlorite 4 veins crosscutting quartz 1 crystals (XPL). C) Dolomite 2-chlorite 4-quartz 4 vein (PPL). D) CL image of dull dolomite 2 crosscut by a later calcite 1 vein. E) Vug developed in quartz 1 crystals partially cemented by rhombic dolomite 2, chlorite 4 and pyrite (PPL). F) CL image of rhombic dolomite crystals in vugs showing a zoned cathodoluminescence.

European regions (i.e. Central French Massif, Alps, German Basin, Ardenne Belt, Sardinia, Arthaud and Matte, 1977; Ziegler, 1988; Faure, 1995; Deroin, 2003; Lago et al., 2004; Depoorter et al., 2014), but not in the CCR, up to now. On the other hand, the latter, although being recognized in the area (Salas et al., 2001), supposes a long-time gap since the end of the Hercynian orogeny (Carboniferous) to let the

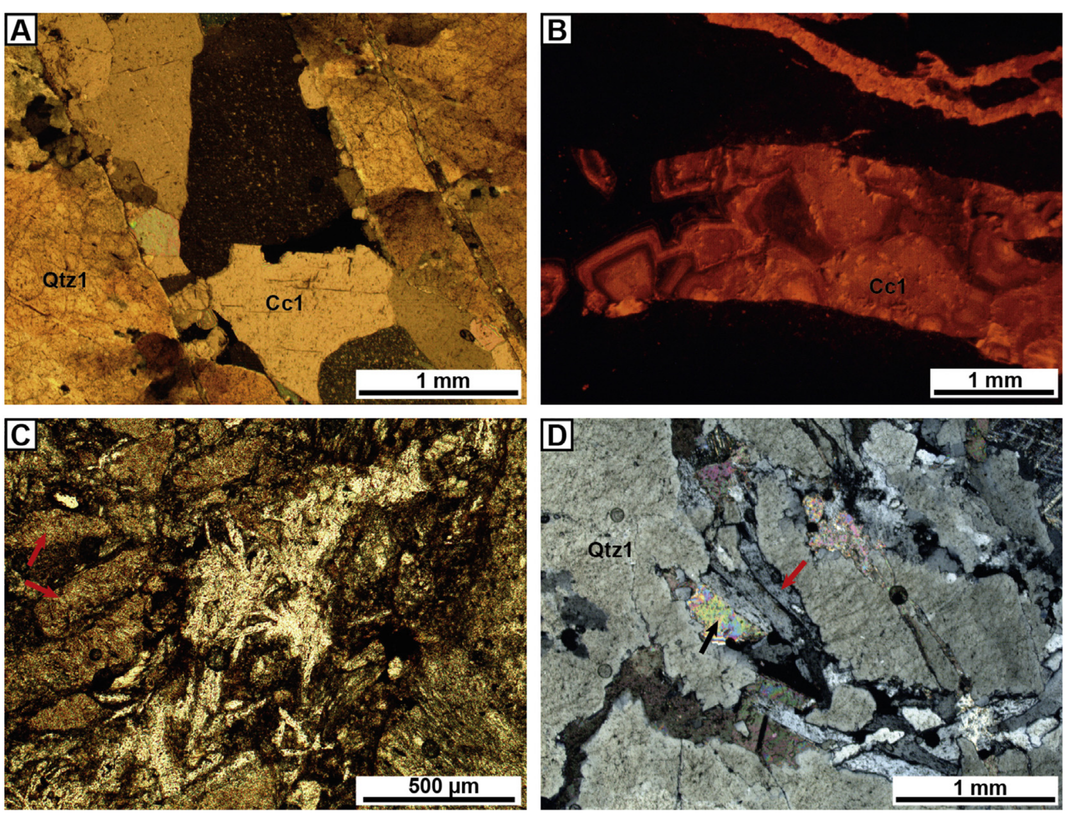

Fig. 11. Microphotographs of the calcite 1-barite paragenesis. A) Fracture cemented by a drusy mosaic of calcite 1 (XPL). B) CL image of a calcite 1 fracture showing their zoned orange pattern. C) Cataclasite formed by phyllite and albite vein clasts (red arrows) cemented by barite (PPL). D) Microfractures between quartz 1 crystals cemented by barite (red arrow) and calcite 1 (black arrow) (XPL). (For interpretation of the references to color in this figure legend, the reader is referred to the web version of this article.)

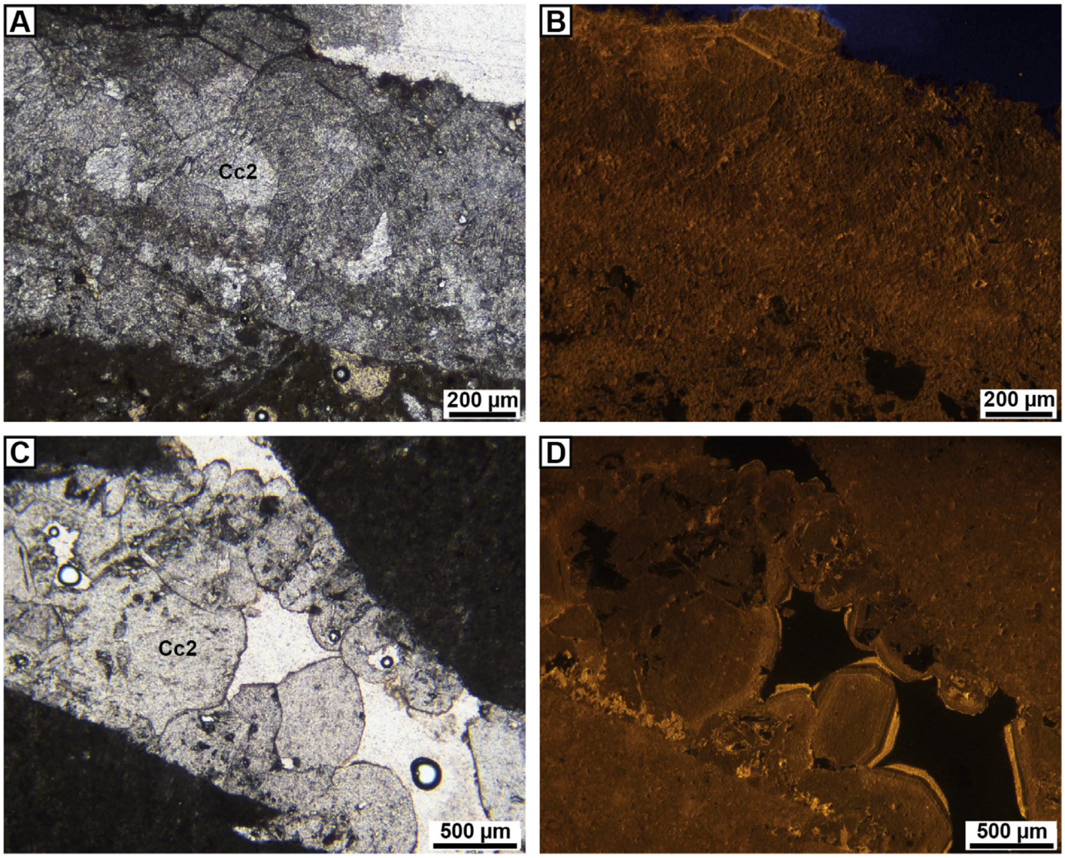

Fig. 12. Microphotographs of the calcite 2 cement. A-B) Plane light and CL image of calcite 2 cement in a fault plane. C-D) Plane light and CL image of calcite 2 cement in joints characterized by rounded crystals and zoned cathodoluminescence.

gradual fluid composition change between the compressional and extensional structures. Moreover, during this time interval, at the end of the Permian, there is a tectonic quiescence stage, registered by the peneplain weathering surface identified in Europe on Paleozoic rocks before the Buntsandstein facies deposition (Gómez-Gras and Ferrer, 1999; Parcerisa et al., 2010). Nevertheless, despite the absence of Permian sedimentation and volcanism in the CCR, Marzo (1979) proposed that the basins delimited by NW-SE faults, where sedimentation of the Buntsandstein facies occurred, were probably formed during the early Permian extension as these facies fossilize the faults. Besides, it is important to highlight that these facies, which unconformably overlay the Ordovician phyllites at the other side of the Llobregat fault (Fig. 1), are not affected by these en-echelon albite veins, thus marking their previous formation. Therefore, we consider that the en-echelon veins and faults cemented by albite are a direct evidence that this early Permian extension also took place in the CCR. Temperature estimates by chlorite thermometry and fluid inclusions indicate a similar range of temperatures than the previous paragenesis, 180–290 °C. However, significant exhumation had already occurred during and after the Hercynian deformation, as synorogenic Carboniferous sandstones (Culm facies) contain clasts made of Ordovician to Tournaisian rocks (Martínez et al., 2016). In fact, as said before, the basal Buntsandstein conglomerates unconformably overlay the Ordovician phyllites, indicating exhumation of the Ordovician rocks during the Permian. Thus, such exhumation implies that the albite paragenesis precipitated from hydrothermal fluids and/or that the geothermal gradient increased highly above 40 °C/km (minimum gradient acquired during metamorphism in the area). Such fluids had higher salinities than the previous ones, from 7.8 to 12.8 wt% NaCl eq., and were Na-rich in order to precipitate albite and Ti-rich in order to precipitate titanite and anatase. Calc-alkaline porphyries intruded the phyllites after Hercynian folding stages but previous to Triassic times (Enrique, 1990). The fluids related to these intrusions were hot and Na-rich, as denoted by the porphyry composition, and also could carry titanium. Moreover, salinities up to 10 wt% NaCl eq. have been observed in veins of epithermal and porphyry deposits related to calc-alkaline magmatism (Heinrich, 2005). Therefore, the progressive entrance of magmatic fluids related to these late-Hercynian granodioritic porphyries may have mixed with the previous metamorphic fluids, explaining the composition, temperature and salinity of these hydrothermal fluids. Also the stop of the prograding metamorphism could explain the salinity increase through the end of dehydration reactions that lowered the salinity by water release (Kenis et al., 2005; Berwouts et al., 2008).

The following dolomite 2-chlorite 4-quartz 4 veins mark a change in the physico-chemical characteristics of the fluid, as the increase in XFe^{3+} in Chl_4 indicates a more oxidizing character of the fluid (Fig. 13) (Lanari et al., 2014; Trincal et al., 2015). Two scenarios can be invoked to produce such a shift in the oxidation conditions: (1) a temperature drop and/or (2) a chemical variation of the rock (Mikucki and Ridley, 1993; Dewaele et al., 2004). Chlorite temperature estimates and fluid inclusions analyses indicate slightly lower precipitation temperatures, between 210 and 280 °C. However, for a fixed bulk rock composition and a temperature decrease of 50 °C, XFe^{3+} only rises 0.06–0.08 (see trends in Fig. 13), being here the shift much higher (0.15–0.35). Thus, an external perturbation is required to significantly affect the redox conditions. Fluid inclusions reveal a fluid mixing line between hot, low to intermediate salinity fluids (recycled from the previous paragenesis) and a subordinate low temperature (140–200 °C) high salinity fluid (Fig. 14). Thus, the change in the oxygen fugacity is probably due to the entrance of a colder and very oxidizing external brine. Applying the equation of Fritz and Smith (1970) for dolomite 2, with $\delta^{18}O$ values between -6.3 and -5.4 ‰VPDB and T between 140 and 280 °C, the $\delta^{18}O$

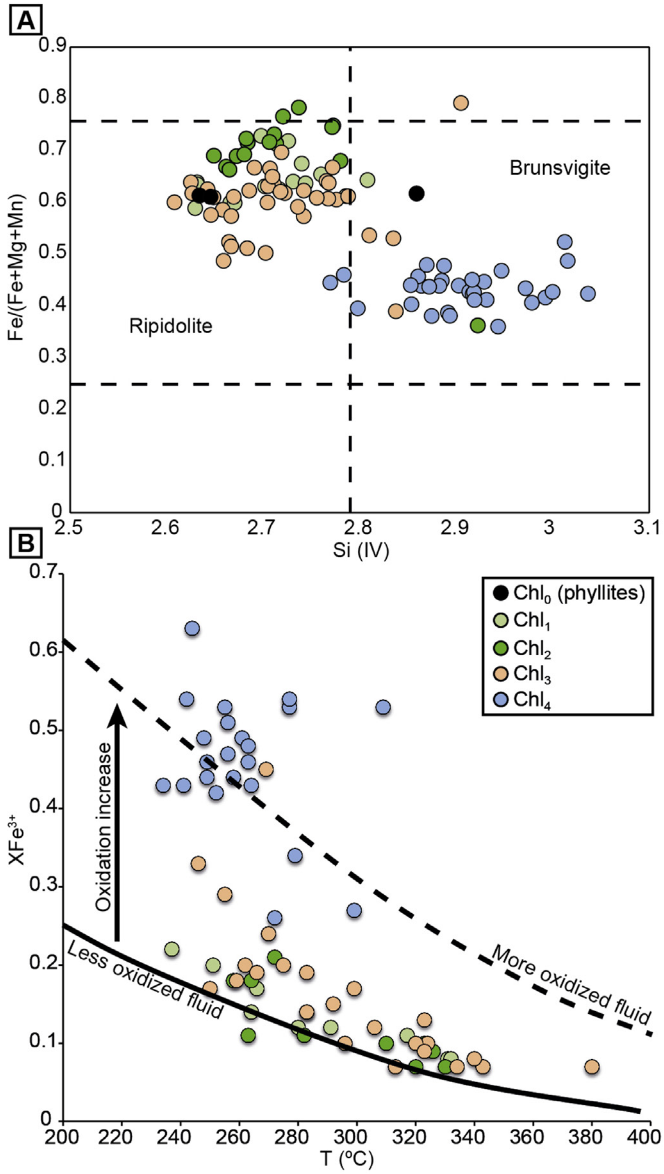

Fig. 13. A) Classification of chlorites according to Foster (1962). B) XFe^{3+} vs. temperature estimated from Vidal et al. (2005, 2006) geothermometer. Two main trends corresponding to two redox conditions of the fluid are observed: one from a less oxidized fluid, defined by chlorites 1 to 3 (continuous line) and one from a more oxidized fluid, defined by chlorites 4 (dashed line).

of the fluids ranges between +7.4 and +19.8 ‰VSMOW. These values confirm that fluids derived or are in equilibrium with metamorphic and igneous rocks and were mixed with a more $\delta^{18}O$-depleted brine (Taylor Jr., 1967, 1977). In turn, the highly ^{13}C-depleted values of dolomite 2 indicates that there was no expulsion of aqueous fluids with CO_2 derived from carbonate rocks from the Paleozoic sequence, which are represented by Ordovician carbonates interbedded with the phyllites and Devonian carbonate rocks (Rumble III et al., 1986). On the contrary, these values may record, on one hand, the production of $\delta^{13}C$-depleted CH_4 during metamorphism and, on the other hand, the production of $\delta^{13}C$-depleted CO_2 during this oxidizing stage, through the oxidation of the carbonaceous material contained in the metapelites and/or the oxidation of $\delta^{13}C$-depleted CH_4 produced during metamorphism (Taylor and O'Neil, 1977; Rumble III et al., 1986). This CO_2 content increase probably caused a change in the XCO_2 gradient, favoring the stability of carbonates in this stage (Mikucki and Ridley, 1993). This increase in CO_2 lowers the water activity and thus may affect the chlorite and XFe^{3+} estimates made with the model of Vidal et al. (2005, 2006). For chl$_4$, the model predicts equilibrium at 264 ± 18 °C for a XFe^{3+} of 0.46 ± 0.08 assuming $aH_2O = 1$, 240 ± 19 °C for a XFe^{3+} of 0.47 ± 0.07 assuming $aH_2O = 0.4$ and 222 ± 17 °C for a XFe^{3+} of 0.48 ± 0.07 assuming $aH_2O = 0.2$ (details in supplementary material S1). This comparison shows that the temperature slightly decreases with decreasing aH_2O, whereas XFe^{3+} is not affected by aH_2O. The predicted decrease of T is however small and remain close to the analytical uncertainty and the model returns values that are in line with the T recorded by the fluid inclusions. Taking into account these observations, dolomite veins were probably formed during the last stages of the early Permian extension during ongoing exhumation (Fig. 16).

Reverse and strike-slip faults observed at mesoscale have been related to the N-S subhorizontal calcite veins according to the similar structural orientation. All these structures, which are a minor phase in the Turó de les Forques, have been related to a compressional event. Vein minerals in this stage are different from previous deformational phases revealing a major change in the fluid composition and origin. Calcite 1 and barite are present instead of chlorite and quartz and, as indicated by the presence of monophasic fluid inclusions (Goldstein and Reynolds, 1994), this mineral paragenesis precipitated at low temperatures, below 50 °C. The presence of barite indicates that the low-temperature fluid contained dissolved SO_4^{2-}, suggesting the presence of seawater or of meteoric water that has remobilized sulfate from evaporites. Besides, this fluid had to interact with Ba-bearing minerals, such as K-feldspars and K-micas (Hanor, 2000), which are main components within the Paleozoic granodiorites and phyllites and the Miocene siliciclastics filling the Neogene basins. These fractures formed after the NE-SW dolomite veins, as indicated by crosscutting relationships, but we cannot settle these structures in time without any doubt. However, the compressional character of these structures leads us to point out that their formation took place either during the Paleogene compressional event or during the minor compressional stage that occurred during the Langhian to early Serravallian. In the former case, reverse faults do not show the common NE-SW Paleogene orientation, but a reactivation of previous discontinuities cannot be excluded. In the latter, reverse and dextral strike-slip faults with similar orientations cemented by calcite and minor barite have been identified in the Burdigalian conglomerates (Parcerisa et al., 2005; Travé and Calvet, 2001; Travé et al., 2009). These calcites have similar $\delta^{18}O$ values to calcite 1 but more positive $\delta^{13}C$. The $\delta^{13}C$-depletion in calcite 1, between -12.7 and -9.7 ‰VPDB, could be caused by organic matter oxidation via sulfate reduction, as could be pointed by the association with barite (Sass et al., 1991), or by the entrance of soil-derived CO_2 (Hudson, 1977).

Finally, the youngest structures identified in the Turó de les Forques correspond to NE-SW and NNW-SSE normal faults affecting both Paleozoic and Miocene rocks, which form gouges and calcite slickenlines, respectively (Fig. 16). The formation of gouges in the NE-SW normal faults affecting the phyllites clearly indicates brittle deformation at very shallow crustal levels (Sibson, 1977). Calcite 2 cement shows a narrow range of $\delta^{13}C$ values consistent with those of the Miocene lacustrine carbonates (−7.7 to −6.5 ‰VPDB), indicating that the fluid was buffered by the Miocene lacustrine carbonates (Tasse and Hesse, 1984; Marshall, 1992). On the other hand, calcite 2 cement is characterized by significant $\delta^{18}O$-depleted values (Fig. 6), which could result from high temperature fluids or low $\delta^{18}O$ groundwaters. High temperature fluids can be ruled out since fluid inclusions in calcite 2 are monophasic and therefore are interpreted to be trapped at temperatures below 50 °C (Goldstein and Reynolds, 1994). Moreover, these fluid inclusion associations formed by uniquely all-liquid fluid inclusions are indicative of their entrapment within the phreatic zone and the lack of heating during burial (Goldstein and Reynolds, 1994). The $\delta^{18}O$ composition of the lacustrine host rocks, −8‰VPDB, is consistent with the $\delta^{18}O$ composition of the Miocene meteoric waters, estimating that

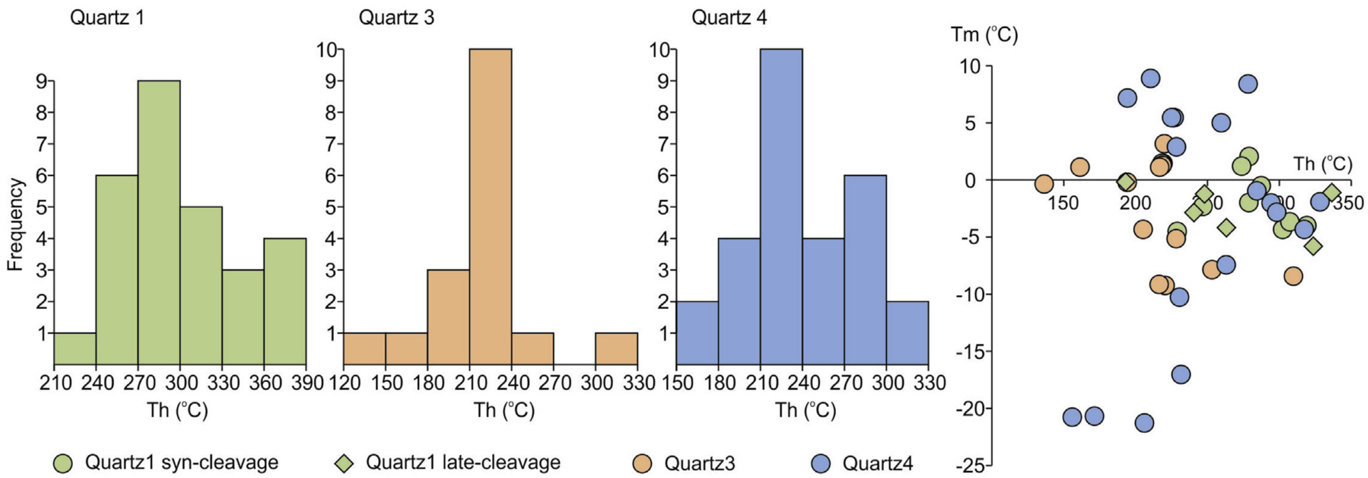

Fig. 14. Homogenization temperatures (T_h) from fluid inclusions obtained for quartz 1, 3 and 4 and T_h vs. T_m plot for quartz 1, 3 and 4.

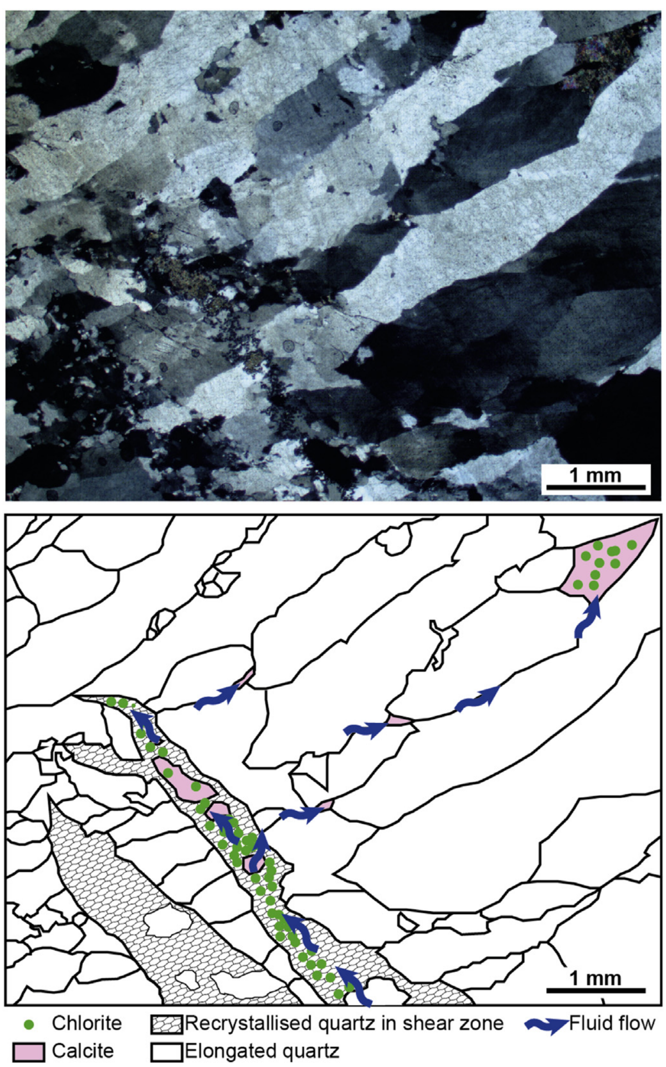

Fig. 15. Pervasive fluid flow during the Hercynian deformation along microshears and intercrystalline boundaries and precipitation in low-pressure areas such as triple points created between elongated quartz crystals.

during the Miocene the Vallès-Penedès basin was only 4° to the south of its current latitude (Smith, 1996) and thus, the $\delta^{18}O$ of precipitation waters was probably similar to current precipitation waters (around −7‰ SMOW, according to Plata (1994) and Redondo and Yélamos (2000)). Thus, applying the equation of Craig (1965), and taking into account this depleted value for groundwaters and the $\delta^{18}O$ of the calcites, a range of fluid temperatures between 34 and 57 °C is obtained. These temperatures are in agreement with the maximum burial depth of Burdigalian sediments in the southern Vallès-Penedès margin (up to 1 km according to Travé et al., 2009), considering a geothermal gradient of 30 °C/km (Juez-Larré, 2003). Calcite 2 cement has similar isotopic values to calcites cementing faults in the Burdigalian clays, sandstones and conglomerates of the surrounding areas (Travé and Calvet, 2001; Travé et al., 2009). These authors also interpreted these calcite cements as precipitated from meteoric waters.

8.2. Structural evolution and fracture development of the Turó de les Forques hill

The Turó de les Forques hill and its associated fracture pattern resulted from a long-lived tectonic history spanning from Carboniferous up to Miocene. Unlike Hercynian quartz veins, albite veins (albite-quartz 3-chlorite 3 ± titanite-anatase) are exclusive from the Ordovician phyllites of the Turó de les Forques. They have not been observed neither in other phyllite outcrops along the CCR nor in any study about deformation and fluids in Mesozoic and Paleozoic rocks along the CCR (Carreras and Santanach, 1975; Cardellach et al., 2002; Tucker and Marshall, 2004; Piqué et al., 2008; Baqués et al., 2012; Cantarero et al., 2014b, c). As a consequence, a specific structural control, different to other areas, had to exist in the Turó de les Forques to be the responsible of these veins. NNW-SSE normal faults were active during the early Permian extensional event (see Marzo (1979), Section 8.1). One of these faults, the Llobregat Fault, limited the Turó de les Forques to the SW following the trace of the current Llobregat River (Fig. 1), and constituted an important paleogeographic limit during the sedimentation of the Buntsandstein controlling its thickness (Marzo, 1979; Anadón et al., 1979). The activity of this fault during the early Permian coupled with the abundance of albite veins in the Turó de les Forques hill allow us to propose that two SW-dipping extensional fault segments, laterally offset, of the Llobregat fault (Fig. 1A), generated a relay zone between the two fault tips (Fig. 17A). The high fracture density, up to 75 fractures/m, and the several fracture orientations are in agreement with fracture patterns described in relay zones in order to accommodate the extension between the two fault tips (Peacock and Sanderson, 1994; Soliva and Benedicto, 2004; Crider and Peacock, 2004). In addition, the interpretation that albite veins precipitated from hydrothermal fluids, produced by the mixing between metamorphic and magmatic fluids, reinforces the interpretation of an existing relay zone during this time, as these zones are preferential pathways for

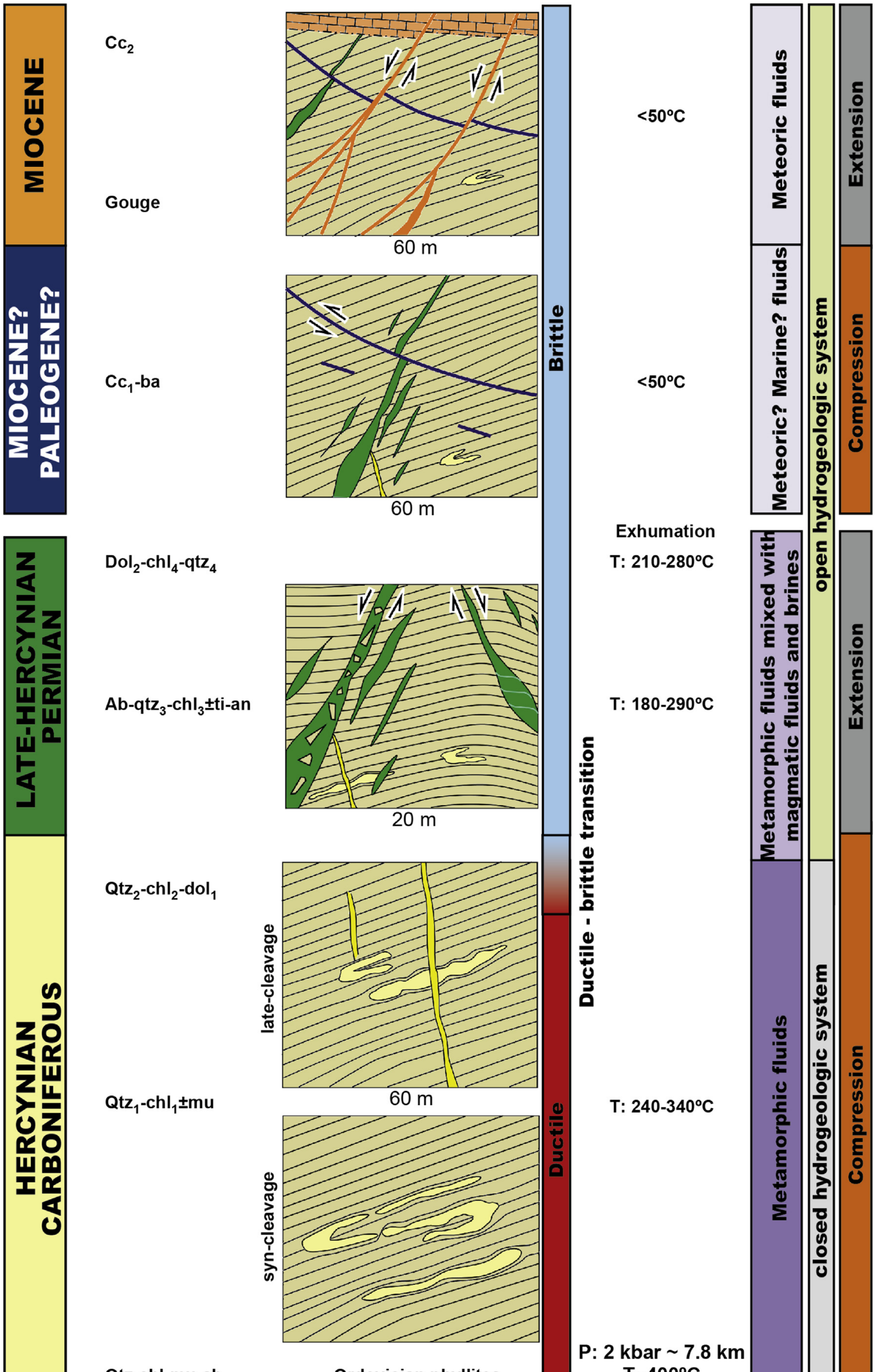

(caption on next page)

Fig. 16. Evolution of deformation from ductile to brittle conditions, from Carboniferous to Miocene times, and its related structures and tectonic regime, mineral paragenesis, temperature and depth conditions, fluid origin and hydrogeologic regime. Qtz: quartz, chl: chlorite, mu: muscovite, ab: albite, dol: dolomite, ti: titanite, an: anatase, cc: calcite, ba: barite.

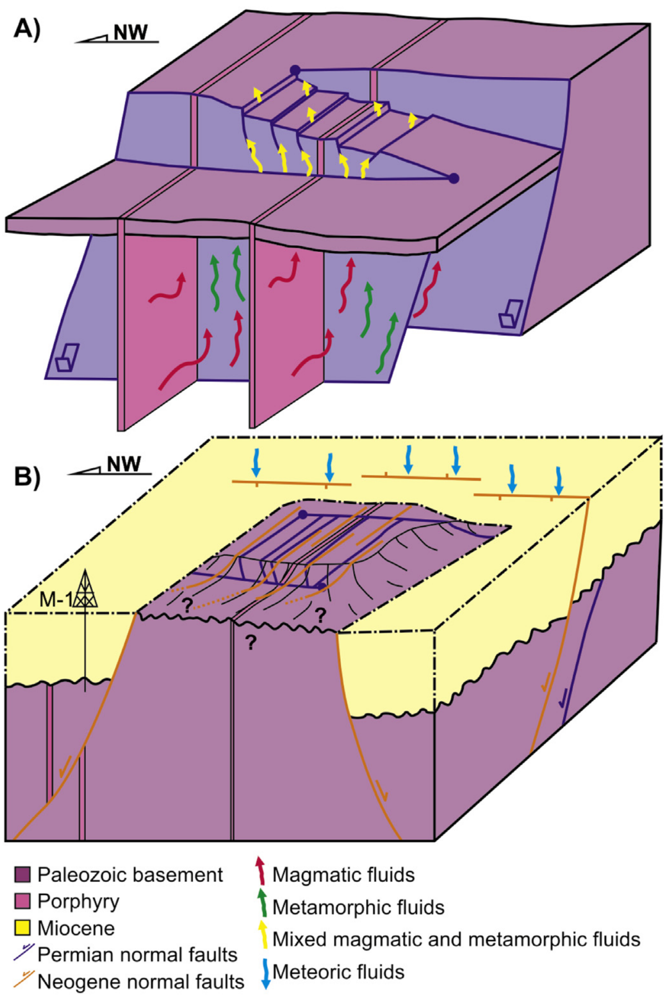

Fig. 17. Structural evolution and fracture development of the Turó de les Forques hill. A) Generation of a relay zone between the two fault segments of the Llobregat fault during the Early Permian. Metamorphic and magmatic fluids ascend along the relay zone. B) Formation of the Turó de les Forques horst during the Miocene. Meteoric waters percolated through the faults. M1: Martorell-1 well.

ascendant fluid flow, including hydrothermal, magmatic and metamorphic fluids, and therefore for cement precipitation (Antonellini and Aydin, 1995; Rotevatn et al., 2007; Fossen and Rotevatn, 2016). Moreover, because of the low porosity and permeability of the phyllites, the hydrothermal upflow was especially focused through the relay fractures that increased the permeability. During the Mesozoic extension, two rifting stages took place in the CCR and deformation was mostly accommodated by the NE-SW faults with minor contribution of the NW-SE transverse fault system (Bartrina et al., 1992). Within the Turó de les Forques and closer areas (Martorell-1 well; Fig. 1), the Mesozoic succession is absent and the Miocene sediments unconformably overlays the Paleozoic rocks (Lanaja, 1987). This fact indicates that the studied area remained as a structural high with no sedimentation or even erosion. The Paleogene compression (middle Eocene - Oligocene) uplifted the whole CCR reactivating previously developed NE-SW extensional faults (Roca, 1994). Within the studied area, this compressional stage could be registered by reverse faults and associated calcite veins. Finally, during the Miocene extension, NE-SW faults generated the current horst and graben geometry of the CCR, which was lately segmented by the reactivation of NW-SE faults. Thus, it is during this phase that the Turó de les Forques acquired its current configuration as an isolated horst (Fig. 17B). The Paleozoic rocks of the horst also remained poorly buried during this extensional event as revealed by the generation of gouges and the precipitation of low temperature cements in the NW-SE normal faults and the thin fluvio-lacustrine Burdigalian sequence (Anadón and Cabrera, 1980; Cabrera, 1981). In contrast, the Martorell-1 well testifies more than 2.2 km of Miocene succession (Lanaja, 1987) denoting the important throw of the NE-SW normal faults and the differential subsidence between the two near areas.

9. Conclusions

The Turó de les Forques horst, formed by Ordovician phyllites, registers a long deformation history that spans from Ordovician to Miocene times that embrace from a ductile regime in the greenschist facies to shallow brittle deformation.

Nine fracture types have been characterized in this horst. Based on petrological and geochemical analyses of their mineral assemblages, the evolution of the fluid flow system was established during the progressive deformation of the sequence constituting the horst:

(1). Syn-cleavage and post-cleavage veins of qtz$_1$-chl$_1$ ± mu and late qtz$_2$-chl$_2$-dol$_1$ formed during the main Hercynian deformation. These cements precipitated from metamorphic fluids, possibly evolved from seawater connate fluids, in a closed hydrological system at temperatures between 240 and 340 °C. The fluid flow system was dominated by a regional channelized system along mesoscopic veins coupled with a local pervasive system through grain boundaries and triple points.

(2). En-echelon vein arrays of ab-qtz$_3$-chl$_3$ ± ti-an and NE-SW normal faults generating breccias mark the change from: 1) ductile to brittle conditions, 2) compressional to extensional tectonics and 3) closed to open hydrologic regime. This paragenesis precipitated from the mixing of metamorphic and magmatic fluids, related to late-Hercynian porphyries, at temperatures between 180 and 290 °C during the early Permian extension.

(3). Dolomite veins (dol$_2$-chl$_4$-qtz$_4$) are possibly associated to the late stage of the early Permian extension. Vein-filling minerals precipitated at 210–280 °C from the mixing of previous fluids with hypersaline external brines in an open hydrological system at more oxidizing conditions.

(4). Reverse faults and cc1-ba veins formed either during the Paleogene compression or during the Langhian to early Serravallian minor compression. Calcite and barite precipitated from meteoric or marine waters in an open hydrological system.

(5). Finally, the Miocene extension is represented by NE-SW normal faults with fault gouges and NW-SE normal faults cemented by calcite 2 that precipitated at temperatures below 50 °C from meteoric fluids in an open basin-scale hydrological system.

The ductile to brittle transition occurred between the change from compressional to extensional tectonics in the early Permian. This transition was produced by the exhumation resulting from the uplift and erosion of the orogen during compression.

The intense albite veining, concentrated exclusively in the Turó de les Forques, together with their shear sense and orientations fits into a kinematic model of a relay ramp between two segments of the Llobregat fault. Such structure, produced during the early Permian collapse of the Hercynian orogen, produced a high-permeability path for the fast upflow of hydrothermal fluids in the low-permeability phyllites.

The outcrop of this early Permian relay zone within the Miocene horst is due to a structural and erosional control. On one hand, the successive deformation phases have reactivated inherited faults, concentrating deformation along the same structures. On the other hand, from Permian up to now, the Turó de les Forques has been a structural high due to its position at the footwall of the NW-SE Permian extensional faults and at the footwall of the NE-SW Miocene extensional faults. As a consequence, the Turó de les Forques has remained as an area of almost no sedimentation and affected by erosion, allowing the exposure of the Permian relay zone.

Supplementary data to this article can be found online at https://doi.org/10.1016/j.gloplacha.2018.03.002.

Acknowledgements

We thank Dr. Zhou and two anonymous referees for their constructive reviews, which helped to improve the quality of the manuscript. The isotopic, Raman, FRX, DRX and electron microprobe analyses were carried out at “Centres Científics i Tecnològics” of the Universitat de Barcelona. This research was performed within the framework of DGICYT Spanish Project CGL2015-66335-C2-1-R and the Grup Consolidat de Recerca “Geologia Sedimentària” (2014SGR-251).

References

Anadón, P., Cabrera, L., 1980. Características de los depósitos lacustres y facies asociadas del Burdigaliense (Mioceno inferior) de la cuenca del Vallès-Penedès. IX Congreso Nacional de Sedimenología, Salamanca, Spain, pp. 261–276.

Anadón, P., Colombo, F., Esteban, M., Marzo, M., Robles, S., Santanach, P., Solé Sugrañés, Ll, 1979. Evolución tectonoestratigráfica de los Catalánides. Acta Geol. Hisp. Homenatge a Lluís Solé i Sabarís 14, 242–270.

Anderson, R., Graham, C.M., Boyce, A.J., Fallick, A.E., 2004. Metamorphic and basin fluids in quartz-carbonate-sulphide veins in the SW Scottish Highlands: a stable isotope and fluid inclusion study. Geofluids 4, 169–185. http://dx.doi.org/10.1111/j.1468-8115.2004.00080.x.

Antonellini, M., Aydin, A., 1995. Effect of faulting on fluid flow in porous sandstones: Geometry and spatial distribution. AAPG Bull. 79, 642–671. http://dx.doi.org/10.1306/8D2B1B60-171E-11D7-8645000102C1865D.

Arthaud, F., Matte, P., 1977. Late Paleozoic strike-slip faulting in southern Europe and northern Africa: result of a right-lateral shear zone between the Appalachians and the Urals. GSA Bull. 88, 1305–1320. http://dx.doi.org/10.1130/0016-7606(1977)88<1305:LPSFIS>2.0.CO;2.

Aydin, A., 2000. Fractures, faults, and hydrocarbon entrapment, migration and flow. Mar. Pet. Geol. 17 (7), 797–814.

Baqués, V., Travé, A., Benedicto, A., Labaume, P., Cantarero, I., 2010. Relationships between carbonate fault rocks and fluid flow regime during propagation of the Neogene extensional faults of the Penedès basin (Catalan Coastal Ranges, NE Spain). J. Geochem. Explor. 106, 24–33. http://dx.doi.org/10.1016/j.gexplo.2009.11.010.

Baqués, V., Travé, A., Roca, E., Marín, M., Cantarero, I., 2012. Geofluid behaviour in successive extensional and compressional events: a case study from the southwestern end of the Vallès-Penedès Fault (Catalan Coastal Ranges, NE Spain). Petrol. Geosci. 18, 17–31. http://dx.doi.org/10.1144/1354-079311-017.

Barnaby, R.J., Rimstidt, J.D., 1989. Redox conditions of calcite cementation interpreted from Mn and Fe contents of authigenic calcite. GSA Bull. 101, 795–804. http://dx.doi.org/10.1130/0016-7606(1989)101<0795:RCOCCI>2.3.CO.

Bartrina, M.T., Cabrera, L., Jurado, M.J., Guimerà, J., Roca, E., 1992. Evolution of the central Catalan margin of the Valencia trough (western Mediterranean). Tectonophysics 203, 219–247.

Berman, R.G., 1991. Thermobarometry using multi-equilibrium calculations; a new technique, with petrological applications. Can. Mineral. 29, 833–855.

Berwouts, I., Van Noorden, M., Muchez, P., Boyce, A.J., Sintubin, M., 2008. Inferring intermediate-scale fluid flow in a heterogeneous metasedimentary multilayer sequence during progressive deformation: evidence from the Monts d'Arrée slate belt (Brittany, France). Geofluids 8, 143–158. http://dx.doi.org/10.1111/j.1468-8123.2008.00213.x.

Birtel, S., Stöckhert, B., 2008. Quartz veins record earthquake-related brittle failure and short term ductile flow in the deep crust. Tectonophysics 457, 53–63. http://dx.doi.org/10.1016/j.tecto.2008.05.018.

Bodnar, R.J., 1993. Revised equation and table for determining the freezing point depression of H2O-NaCl solutions. Geochim. Cosmochim. Acta 57, 683–684. http://dx.doi.org/10.1016/0016-7037(93)90378-A.

Cabrera, L., 1981. Influencia de la tectónica en la sedimentación continental de la cuenca del Valles-Penedes (provincia de Barcelona, España) durante el Mioceno inferior. Acta Geol. Hisp. 16, 165–171.

Cantarero, I., Lanari, P., Vidal, O., Alías, G., Travé, A., Baqués, V., 2012. Evolution of the Vallès fault from chlorite and mica equilibrium. Geo-Temas 13, 770–773.

Cantarero, I., Zafra, C.J., Travé, A., Martín-martín, J.D., Baqués, V., Playà, E., 2014a. Fracturing and cementation of shallow buried Miocene proximal alluvial fan deposits. Mar. Pet. Geol. 55, 87–99.

Cantarero, I., Lanari, P., Vidal, O., Alías, G., Travé, A., Baqués, V., 2014b. Long-term fluid circulation in extensional faults in the central Catalan Coastal Ranges: P–T constraints from neoformed chlorite and K-white mica. Int. J. Earth Sci. 103, 165–188. http://dx.doi.org/10.1007/s00531-013-0963-8.

Cantarero, I., Travé, A., Alías, G., Baqués, V., 2014c. Polyphasic hydrothermal and meteoric fluid regimes during the growth of a segmented fault involving crystalline and carbonate rocks (Barcelona Plain, NE Spain). Geofluids 14, 20–44. http://dx.doi.org/10.1111/gfl.12021.

Cardellach, E., Canals, À., Grandia, F., 2002. Recurrent hydrothermal activity induced by successive extensional episodes: the case of the Berta F-(Pb-Zn) vein system (NE Spain). Ore Geol. Rev. 22, 133–141. http://dx.doi.org/10.1016/S0169-1368(02)00112-9.

Carreras, J., Santanach, P., 1975. Precisiones acerca de la significación petrológica y estructural de las rocas gneísicas y cataclásticas del Maresme (prov. de Barcelona). Acta Geol. Hisp. X, 49–54.

Connolly, J.A.D., 1997. Devolatilization-generated fluid pressure and deformation-propagated fluid flow during prograde regional metamorphism. J. Geophys. Res. 102, 18149–18173. http://dx.doi.org/10.1029/97jb00731.

Connolly, J.A.D., 2010. The mechanics of metamorphic fluid expulsion. Elements 6, 165–172. http://dx.doi.org/10.2113/gselements.6.3.165.

Craig, H., 1965. The measurements of oxygen isotope paleotemperatures. In: Tongiorgi, E. (Ed.), Stable Isotopes in Oceanographic Studies and Paleotemperatures. Consiglio Nazionale delle Richerche, Laboratorio di Geologia Nucleare, Pisa, pp. 161–182.

Crider, J.G., Peacock, D.C.P., 2004. Initiation of brittle faults in the upper crust: a review of field observations. J. Struct. Geol. 26, 691–707. http://dx.doi.org/10.1016/j.jsg.2003.07.007.

Cruset, D., Cantarero, I., Travé, A., Vergés, J., John, C.M., 2016. Crestal graben fluid evolution during growth of the Puig-reig anticline (South Pyrenean fold and thrust belt). J. Geodyn. 101, 30–50. http://dx.doi.org/10.1016/j.jog.2016.05.004.

Dee, S.J., Roberts, S., 1993. Late-kinematic gold mineralization during regional uplift and the role of nitrogen – an example from the La Codosera area, W Spain. Mineral. Mag. 57, 437–450.

Deming, D., 1994. Fluid Flow and Heat Transport in the Upper Continental Crust. In: Parnell, J. (Ed.), Geofluids: Origin. Geological Society Special Publication, Migration and Evolution of Fluids in Sedimentary Basins, pp. 27–42.

Depoorter, S., Jacques, D., Piessens, K., Muchez, P., Sintubin, M., 2014. The Mousny massive quartz occurrence - the vestige of a late-orogenic dilational jog in the High-Ardenne slate belt (Belgium). Geol. Belg. 17 (3–4), 293–310.

Deroin, J.P., 2003. Le bassin permien de Blanzy-le-Creusot et ses bordures carbonifères. Bull. Inf. Géol. Bassin Paris 40, 3–28.

Dewaele, S., Muchez, P., Banks, D.A., 2004. Fluid evolution along multistage composite fault systems at the southern margin of the Lower Palaeozoic Anglo-Brabant fold belt, Belgium. Geofluids 4, 341–356. http://dx.doi.org/10.1111/j.1468-8123.2004.00096.x.

Duddy, I.R., Green, P.F., Bray, R.J., Hegarty, K.A., 1994. Recognition of the thermal effects of fluid flow in sedimentary basins. In: Parnell, J. (Ed.), Geofluids: Origin, Migration and Evolution of Fluids in Sedimentary Basins. 78. Geological Society Special Publication, pp. 325–345.

Enrique, P., 1990. The Hercynian intrusive rocks of the Catalonian Coastal Ranges (NE Spain). Acta Geol. Hisp. 25, 39–64.

Faure, M., 1995. Late orogenic carboniferous extensions in the Variscan French Massif Central. Tectonics 14, 132–153. http://dx.doi.org/10.1029/94TC02021.

Ferry, J.M., Dipple, G.M., 1991. Fluid flow, mineral reactions, and metasomatism. Geology 19, 211–214.

Fossen, H., Rotevatn, A., 2016. Fault linkage and relay structures in extensional settings-a review. Earth Sci. Rev. 154, 14–28. http://dx.doi.org/10.1016/j.earscirev.2015.11.014.

Foster, M.D., 1962. Interpretation of the composition and a classification of the chlorites. US Geol. Surv. Prof. Pap. 414-A, 1–33.

Fritz, P., Smith, D.G.W., 1970. The isotopic composition of secondary dolomites. Geochim. Cosmochim. Acta 34, 1161–1173. http://dx.doi.org/10.1016/0016-7037(70)90056-6.

Fyfe, W.S., Price, N.J., Thompson, A.B., 1978. Fluids in the Earth's crust. Their significance in metamorphic, tectonic and chemical transport processes. In: Developments in Geochemistry. 1 Elsevier Scientific Publishing Company, Amsterdam (383 p).

Garven, G., 1989. A hydrogeologic model for the formation of the giant oil sands deposits of the western Canada sedimentary basin. Am. J. Sci. 289, 105–166.

Gaspar-Escribano, J.M., Garcia-Castellanos, D., Roca, E., Cloetingh, S., 2004. Cenozoic vertical motions of the Catalan Coastal Ranges (NE Spain): the role of tectonics, isostasy, and surface transport. Tectonics 23, TC1004. http://dx.doi.org/10.1029/2003TC001511.

Ghisetti, F., Kirschner, D.L., Vezzani, L., Agosta, F., 2001. Stable isotope evidence for contrasting paleofluid circulation in thrust faults and normal faults of the central Apennines, Italy. J. Geophys. Res. 106, 8811–8825. http://dx.doi.org/10.1029/2000JB900377.

Gil Ibarguchi, J.I., Julivert, M., 1988. Petrología de la aureola metamórfica de la granodiorita de Barcelona en la sierra de Collcerola (Tibidabo). Estud. Geol. 44, 353–374.

Goldstein, R.H., Reynolds, T.J., 1994. Systematics of fluid inclusions in diagenetic minerals. SEPM Short. Course Notes 31, 198.

Gómez-Gras, D., Ferrer, C., 1999. Caracterización petrológica de perfiles de meteorización antiguos desarrollados en granitos tardihercínicos de la Cordillera Costero Catalana. Rev. Soc. Geol. Esp. 12, 281–299.

Guimerà, J., 1984. Palaeogene evolution of deformation in the northeastern Iberian Peninsula. Geol. Mag. 121 (5), 413–420.

Hanor, J.S., 1994. Origin of saline fluids in sedimentary basins. In: Geofluids: Origin, Migration and Evolution of Fluids in Sedimentary Basins. Geological Society Special Publication, pp. 151–174. http://dx.doi.org/10.1144/GSL.SP.1994.078.01.13.

Hanor, J.S., 2000. Barite-Celestine geochemistry and environments of formation. Rev. Mineral. Geochem. 40, 193–275. http://dx.doi.org/10.2138/rmg.2000.40.4.

Heinrich, C.A., 2005. The physical and chemical evolution of low-salinity magmatic fluids at the porphyry to epithermal transition: a thermodynamic study. Mineral. Deposita 39, 864–889. http://dx.doi.org/10.1007/s00126-004-0461-9.

Hudson, J.D., 1977. Stable isotopes and limestone lithification. J. Geol. Soc. London. 133, 637–660. http://dx.doi.org/10.1144/gsjgs.133.6.0637.

Imber, J., Holdsworth, R.E., Butler, C.A., 2001. A reappraisal of the Sibson–Scholz fault zone model: the nature of the frictional to viscous ("brittle-ductile") transition along a long-lived, crustal-scale fault, Outer Hebrides, Scotland. Tectonics 20, 601–624.

Juez-Larré, J., 2003. Post Late Paleozoic tectonothermal evolution of the northeastern margin of Iberia, assessed by fission-track and (U-Th)/He analyses. In: A Case History From the Catalan Coastal Ranges. Ph.D. Thesis. Vrije Universiteit, Amsterdam.

Julivert, M., Duran, H., 1990a. The Hercynian structure of the Catalonian Coastal Ranges (NE Spain). Acta Geol. Hisp. 25, 13–21.

Julivert, M., Duran, H., 1990b. Paleozoic stratigraphy of the central and northern part of the Catalonian Coastal Ranges (NE Spain). Acta Geol. Hisp. 25, 3–12.

Kenis, I., Muchez, P., Verhaert, G., Boyce, A.J., Sintubin, M., 2005. Fluid evolution during burial and Variscan deformation in the Lower Devonian rocks of the High-Ardenne slate belt (Belgium): sources and causes of high-salinity and C-O-H-N fluids. Contrib. Mineral. Petrol. 150, 102–118.

Kruhl, J.H., Wirth, R., Morales, L.F.G., 2013. Quartz grain boundaries as fluid pathways in metamorphic rocks. J. Geophys. Res. 118, 1957–1967. http://dx.doi.org/10.1002/jgrb.50099.

Labaume, P., Moretti, I., 2001. Diagenesis-dependence of cataclastic thrust fault zone sealing in sandstones. Example from the Bolivian Sub-Andean Zone. J. Struct. Geol. 23, 1659–1675. http://dx.doi.org/10.1016/S0191-8141(01)00024-4.

Lacroix, B., Charpentier, D., Buatier, M., Vennemann, T., Labaume, P., Adatte, T., Travé, A., Dubois, M., 2012. Formation of chlorite during thrust fault reactivation. Record of fluid origin and P-T conditions in the Monte Perdido thrust fault (southern Pyrenees). Contrib. Mineral. Petrol. 163, 1083–1102. http://dx.doi.org/10.1007/s00410-011-0718-0.

Lago, M., Arranz, E., Pocoví, A., Galé, C., Gil-Imaz, A., 2004. Permian magmatism and basin dynamics in the southern Pyrenees: a record of the transition from late Variscan transtension to the early Alpine extension. In: Wilson, M., Neumann, E., Davies, G., Timmerman, M., Heeremans, M., Larsen, B. (Eds.), Permo-Carboniferous Magmatism and Rifting in Europe. Geological Society, London, Special Publications, pp. 439–464. http://dx.doi.org/10.1144/gsl.sp.2004.223.01.19.

Lanaja, J.M., 1987. Contribución de la exploración petrolífera al conocimiento de la Geología de España. IGME, Ministerio Industria Energía, Madrid (465 pp).

Lanari, P., 2012. Micro-cartographie P-T-e dans les roches métamorphiques Applications aux Alpes et à l'Himalaya. Ph.D. Thesis. Université de Grenoble, France.

Lanari, P., Guillot, S., Schwartz, S., Vidal, O., Tricart, P., Riel, N., Beyssac, O., 2012. Diachronous evolution of the alpine continental subduction wedge: evidence from P-T estimates in the Briançonnais zone houillère (France – Western Alps). J. Geodyn. 56–57, 39–54. http://dx.doi.org/10.1016/j.jog.2011.09.006.

Lanari, P., Wagner, T., Vidal, O., 2014. A thermodynamic model for di-trioctahedral chlorite from experimental and natural data in the system MgO-FeO-Al_2O_3-SiO_2-H_2O: applications to P-T sections and geothermometry. Contrib. Mineral. Petrol. 167, 1–19. http://dx.doi.org/10.1007/s00410-014-0968-8.

Marquer, D., Burkhard, M., 1992. Fluid circulation, progressive deformation and mass-transfer processes in the upper crust: the example of basement-cover relationships in the external crystalline Massifs, Switzerland. J. Struct. Geol. 14, 1047–1057. http://dx.doi.org/10.1016/0191-8141(92)90035-U.

Marshall, J.D., 1992. Climatic and oceanographic isotopic signals from the carbonate rock record and their preservation. Geol. Mag. 129, 143. http://dx.doi.org/10.1017/S0016756800008244.

Martínez, F.J., Dietsch, C., Aleinikoff, J., Cirés, J., Arboleya, M.L., Reche, J., Gómez-Gras, D., 2016. Provenance, age, and tectonic evolution of Variscan flysch, southeastern France and northeastern Spain, based on zircon geochronology. GSA Bull. 128, 842–859. http://dx.doi.org/10.1130/B31316.1.

Marzo, M., 1979. El Bundsandstein de los Catalánides: Estratigrafía y procesos sedimentarios. Ph.D. Thesis. Universitat de Barcelona, Spain.

Matte, P., 2001. The Variscan collage and orogeny (480 ± 290 Ma) and the tectonic de definition of the Armorica microplate: a review. Terra Nova 13, 122–128.

McCrea, J.M., 1950. On the isotopic chemistry of carbonates and a paleotemperature scale. J. Chem. Phys. 18, 849–857. http://dx.doi.org/10.1063/1.1747785.

Mikucki, E.J., Ridley, J.R., 1993. The hydrothermal fluid of Archaean lode-gold deposits at different metamorphic grade: compositional constraints from ore and wallrock alteration assemblages. Mineral. Deposita 28, 469–481.

Miller, J. a, Cartwright, I., 2006. Albite vein formation during exhumation of high-pressure terranes: a case study from alpine Corsica. J. Metamorph. Geol. 24, 409–428. http://dx.doi.org/10.1111/j.1525-1314.2006.00645.x.

Moore, C.H., 1989. Carbonate Diagenesis and Porosity. Developments in Sedimentology. 46. Elsevier, pp. 338.

Nesbitt, B.E., Muehlenbachs, K., 1989. Origins and movement of fluids during deformation and metamorphism in the Canadian Cordillera. Science 245, 733–736. http://dx.doi.org/10.1126/science.245.4919.733.

Oliver, N.H.S., 1996. Review and classification of structural controls on fluid flow during regional metamorphism. J. Metamorph. Geol. 14, 477–492. http://dx.doi.org/10.1046/j.1525-1314.1996.00347.x.

Oliver, N.H.S., 2001. Linking of regional and local hydrothermal systems in the mid-crust by shearing and faulting. Tectonophysics 335, 147–161. http://dx.doi.org/10.1016/S0040-1951(01)00054-3.

Parcerisa, D., Gómez-Gras, D., Travé, A., 2005. A model of early calcite cementation in alluvial fans: evidence from the Burdigalian sandstones and limestones of the Vallès–Penedès half-graben (NE Spain). Sediment. Geol. 178, 197–217. http://dx.doi.org/10.1016/j.sedgeo.2005.04.004.

Parcerisa, D., Gómez-Gras, D., Travé, A., Martín-Martín, J.D., 2006. Fe and Mn in calcites cementing red beds: a record of oxidation–reduction conditions. Examples from the Catalan Coastal Ranges (NE Spain). J. Geochem. Explor. 89, 318–321. http://dx.doi.org/10.1016/j.gexplo.2005.11.081.

Parcerisa, D., Thiry, M., Schmitt, J.M., 2010. Albitisation related to the triassic unconformity in igneous rocks of the morvan massif (France). Int. J. Earth Sci. 99, 527–544. http://dx.doi.org/10.1007/s00531-008-0405-1.

Peacock, D.C.P., Sanderson, D.J., 1994. Geometry and deveopment of relay ramps in normal fault systems. AAPG Bull. 78, 147–165. http://dx.doi.org/10.1306/BDFF9046-1718-11D7-8645000102C1865D.

Piqué, À., Canals, À., Grandia, F., Banks, D.A., 2008. Mesozoic fluorite veins in NE Spain record regional base metal-rich brine circulation through basin and basement during extensional events. Chem. Geol. 257, 139–152. http://dx.doi.org/10.1016/j.chemgeo.2008.08.028.

Pitcairn, I.K., Skelton, A.D.L., Broman, C., Arghe, F., Boyce, A., 2010. Structurally focused fluid flow during orogenesis: the Islay anticline, SW Highlands, Scotland. J. Geol. Soc. London 167, 659–674. http://dx.doi.org/10.1144/0016-76492009-135.

Plata, A., 1994. Composición isotópica de las precipitaciones y aguas subterráneas de la Península Ibérica. Centro de Estudios y Experimentación de Obras Públicas. Madrid, Pub. M-39. pp. 1–139.

Putnis, A., 2002. Mineral replacement reactions: from macroscopic observations to microscopic mechanisms. Mineral. Mag. 66 (5), 689–708.

Redondo, R., Yélamos, J.G., 2000. Hidrogeoquímica convencional e isotópica de las aguas carbonáticas de Cataluña. Geogaceta 28, 121–124.

Roca, E., 1994. La evolución geodinámica de la Cuenca Catalano-Balear y áreas adyacentes desde el Mesozoico hasta la actualidad. Acta Geol. Hisp. 29, 3–25.

Roca, E., Guimerà, J., 1992. The Neogene structure of the eastern Iberian margin – structural constraints on the crustal evolution of the Valencia trough (western Mediterranean). Tectonophysics 203, 203–218. http://dx.doi.org/10.1016/0040-1951(92)90224-T.

Rotevatn, A., Fossen, H., Hesthammer, J., Aas, T.E., Howell, J.A., 2007. Are relay ramps conduits for fluid flow? Structural analysis of a relay ramp in Arches National Park, Utah. In: Lonergan, L., Jolly, R.J.H., Rawnsley, K., Sanderson, D.J. (Eds.), Fractured Reservoirs. Geological Society, London, Special Publications, pp. 55–71. http://dx.doi.org/10.1144/GSL.SP.2007.270.01.04.

Rumble III, D., Duke, E.F., Hoering, T.L., 1986. Hydrothermal graphite in New Hampshire: evidence of carbon mobility during regional metamorphism. Geology 14, 452–455. http://dx.doi.org/10.1130/0091-7613(1986)14 < 452:HGINHE > 2.0.CO;2.

Salas, R., Guimerà, J., Mas, R., Martín-Closas, C., Meléndez, A., Alonso, A., 2001. Evolution of the mesozoic Central Iberian rift system and its cainozoic inversion (Iberian chain). In: Ziegler, P.A., Cavazza, W., Robertson, A.H.F., Crasquin-Soleau, S. (Eds.), Peri-Tethys Memoir 6: Peri-Tethyan Rift/Wrench Basins and Passive Margins. Mem. Mus. natn. Hist. nat, pp. 145–186.

Santanach, P., Casas, J.M., Gratacós, O., Liesa, M., Muñoz, J.A., Sàbat, F., 2011. Variscan and alpine structure of the hills of Barcelona: geology in an urban area. J. Iber. Geol. 37, 121–136. http://dx.doi.org/10.5209/rev.

Sass, E., Bein, A., Almogi-Labin, A., 1991. Oxygen-isotope composition of diagenetic calcite in organic-rich rocks: evidence for 18O depletion in marine anaerobic pore water. Geology 19, 839–842. http://dx.doi.org/10.1130/0091-7613(1991)019 < 0839:OICODC > 2.3.CO.

Shepherd, T.J., Bottrell, S.H., Miller, M.F., 1991. Fluid inclusion volatiles as an exploration guide to black shale-hosted gold deposits, Dolgellau gold belt, North Wales, UK. J. Geochem. Explor. 42, 5–24. http://dx.doi.org/10.1016/0375-6742(91)90058-3.

Sibson, R.H., 1977. Fault rocks and fault mechanisms. Geol. Soc. London 133, 191–213.

Sibson, R.H., Scott, J., 1998. Stress/fault controls on the containment and release of overpressured fluids: examples from gold-quartz vein systems in Juneau, Alaska; Victoria, Australia and Otago, New Zealand. Ore Geol. Rev. 13, 293–306.

Smith, A.G., 1996. Cenozoic latitudes, positions and topography of the Iberian Peninsula. In: Friend, P.F., Dabrio, C.J. (Eds.), Tertiary Basins of Spain: The Stratigraphic Record of Crustal Kinematics, World and Regional Geology. 6. Cambridge University Press, Cambridge, pp. 6–8.

Smith, M., Yardley, B., 1999a. Fluid evolution during metamorphism of the Otago Schist, New Zealand: (I) Evidence from fluid inclusions. J. Metamorph. Geol. 17, 173–186. http://dx.doi.org/10.1046/j.1525-1314.1999.00189.x.

Smith, M.P., Yardley, B.W.D., 1999b. Fluid evolution during metamorphism of the Otago Schist, New Zealand: (II) influence of detrital apatite on fluid salinity. J. Metamorph. Geol. 17, 187–193. http://dx.doi.org/10.1046/j.1525-1314.1999.00190.x.

Soliva, R., Benedicto, A., 2004. A linkage criterion for segmented normal faults. J. Struct. Geol. 26, 2251–2267. http://dx.doi.org/10.1016/j.jsg.2004.06.008.

Tasse, N., Hesse, R., 1984. Origin and significance of complex authigenic carbonates in Cretaceous black shales of the Western Alps. J. Sediment. Petrol. 54, 1012–1027.

Taylor Jr., H.P., 1967. Oxygen isotope studies of hydrothermal mineral deposits. In: Barnes, H.L. (Ed.), Geochemistry of Hydrothermal Ore Deposits. Holt, Rinehart and Winston, pp. 670.

Taylor Jr., H.P., 1977. Water/rock interactions and the origin of H_2O in granitic batholiths. J. Geol. Soc. London 133, 509–558.

Taylor, B.E., O'Neil, J.R., 1977. Stable isotope studies of metasomatic Ca-Fe-Al-Si skarns and associated metamorphic and igneous rocks, Osgood Mountains, Nevada. Contrib. Mineral. Petrol. 63, 1–49. http://dx.doi.org/10.1007/BF00371674.

Travé, A., Calvet, F., 2001. Syn-rift geofluids in fractures related to the early-middle Miocene evolution of the Vallès-Penedès half-graben (NE Spain). Tectonophysics 336,

101–120.
Travé, A., Calvet, F., Soler, A., Labaume, P., 1998. Fracturing and fluid migration during Palaeogene compression and Neogene extension in the Catalan Coastal Ranges, Spain. Sedimentology 45, 1063–1082.
Travé, A., Roca, E., Playà, E., Parcerisa, D., Gómez-Gras, D., Martín-Martín, J.D., 2009. Migration of Mn-rich fluids through normal faults and fine-grained terrigenous sediments during early development of the Neogene Vallès-Penedès half-graben (NE Spain). Geofluids 9, 303–320. http://dx.doi.org/10.1111/j.1468-8123.2009.00258.x.
Trincal, V., Lanari, P., Buatier, M., Lacroix, B., Charpentier, D., Labaume, P., Muñoz, M., 2015. Temperature micro-mapping in oscillatory-zoned chlorite: application to study of a green-schist facies fault zone in the Pyrenean Axial Zone (Spain). Am. Mineral. 100, 2468–2483. http://dx.doi.org/10.2138/am-2015-5217.
Tucker, M., Marshall, J., 2004. Diagenesis and geochemistry of Upper Muschelkalk (Triassic) buildups and associated facies in Catalonia (NE. Spain): a paper dedicated to Francesc Calvet. Geol. Acta 2, 257–269.
Van Den Kerkhof, A., Thiéry, R., 2001. Carbonic inclusions. Lithos 55, 49–68. http://dx.doi.org/10.1016/S0024-4937(00)00038-4.
Van Noten, K., Hilgers, C., Urai, J.L., Sintubin, M., 2008. Late burial to early tectonic quartz veins in the periphery of the High-Ardenne slate belt (Rursee, North Eifel, Germany). Geol. Belg. 11 (3–4), 179–198.
Van Noten, K., Muchez, P., Sintubin, M., 2011. Stress-state evolution of the brittle upper crust during compressional tectonic inversion as defined by successive quartz vein-types (High-Ardenne slate belt, Germany). J. Geol. Soc. London 168 (2), 407–422.
Vergés, J., García-Senz, J., Ziegler, P.A., et al., 2001. Mesozoic evolution and Cainozoic inversion of the Pyrenean rift. In: Peri-Tethys Memoir 6: Peri-Tethyan Rift/Wrench Basins and Passive Margins. Mém. Mus. natn Hist. nat. 186. pp. 187–212.
Vidal, O., Dubacq, B., 2009. Thermodynamic modelling of clay dehydration, stability and compositional evolution with temperature, pressure and H2O activity. Geochim. Cosmochim. Acta 73, 6544–6564. http://dx.doi.org/10.1016/j.gca.2009.07.035.
Vidal, O., Parra, T., Trotet, F., 2001. A thermodynamic model for Fe-Mg aluminous chlorite using data from phase equilibrium experiments and natural pelitic assemblages in the 100° to 600° C, 1 to 25 kb range. Am. J. Sci. 301, 557–592. http://dx.doi.org/10.2475/ajs.301.6.557.
Vidal, O., Parra, T., Vieillard, P., 2005. Thermodynamic properties of the Tschermak solid solution in Fe-chlorite: application to natural examples and possible role of oxidation. Am. Mineral. 90, 347–358. http://dx.doi.org/10.2138/am.2005.1554.
Vidal, O., De Andrade, V., Lewin, E., Munoz, M., Parra, T., Pascarelli, S., 2006. P-T-deformation-Fe^{3+}/Fe^{2+} mapping at the thin section scale and comparison with XANES mapping: application to a garnet-bearing metapelite from the Sambagawa metamorphic belt (Japan). J. Metamorph. Geol. 24, 669–683. http://dx.doi.org/10.1111/j.1525-1314.2006.00661.x.
Vidal, O., Lanari, P., Muñoz, M., Bourdelle, F., de Andrade, V., 2016. Deciphering temperature, pressure, and oxygen activity conditions of chlorite formation. Clay Miner. 51, 615–633. http://dx.doi.org/10.1180/claymin.2016.051.4.06.
Vilà, M., Pin, C., 2016. Geochemistry and Nd isotope signature of the Collserola range Palaeozoic succession (NE Iberia): Gondwana heritage and pre-Mesozoic geodynamic evolution. Geol. Mag. 153, 643–662. http://dx.doi.org/10.1017/S0016756815000837.
Walther, J.V., Orville, P.M., 1982. Volatile production and transport in regional metamorphism. Contrib. Mineral. Petrol. 79, 252–257. http://dx.doi.org/10.1007/BF00371516.
Wood, B.J., Walther, J.V., 1986. fluid flow during metamorphism and its implications for fluid-rock ratios. In: Walther, J.V., Wood, B.J. (Eds.), Fluid-Rock Interactions during Metamorphism. Advances in Physical Geochemistry. 5 Springer, New York, NY.
Yardley, B.W.D., 1986. Fluid migration and veining in the Connemara schists, Ireland. In: Walther, J.V., Wood, B.J. (Eds.), Fluid–Rock Interactions during Metamorphism. Springer Verlag, New York, pp. 109–131.
Yardley, B.W.D., 1997. The evolution of fluids through the metamorphic cycle. In: Jamtveit, B., Yardley, B.W.D. (Eds.), Fluid Flow and Transport in Rocks: Mechanisms and Effects. Chapman & Hall, London, pp. 99–121.
Yardley, B.W.D., Graham, J.T., 2002. The origins of salinity in metamorphic fluids. Geofluids 2, 249–256. http://dx.doi.org/10.1046/j.1468-8123.2002.00042.x.
Zhang, R.Y., Liou, J.G., Zheng, Y.F., Fu, B., 2003. Transition of UHP eclogites to gneissic rocks of low-amphibolite facies during exhumation: evidence from the Dabie terrane, central China. Lithos 70, 269–291. http://dx.doi.org/10.1016/S0024-4937(03)00102-6.
Ziegler, P.a, 1988. Evolution of the Arctic-North Atlantic and the western Tethys. AAPG Mem. http://dx.doi.org/10.1306/M43478.